Cell Reports
Medicine

Article

PRMT1 promotes pancreatic cancer development and resistance to chemotherapy

Graphical abstract

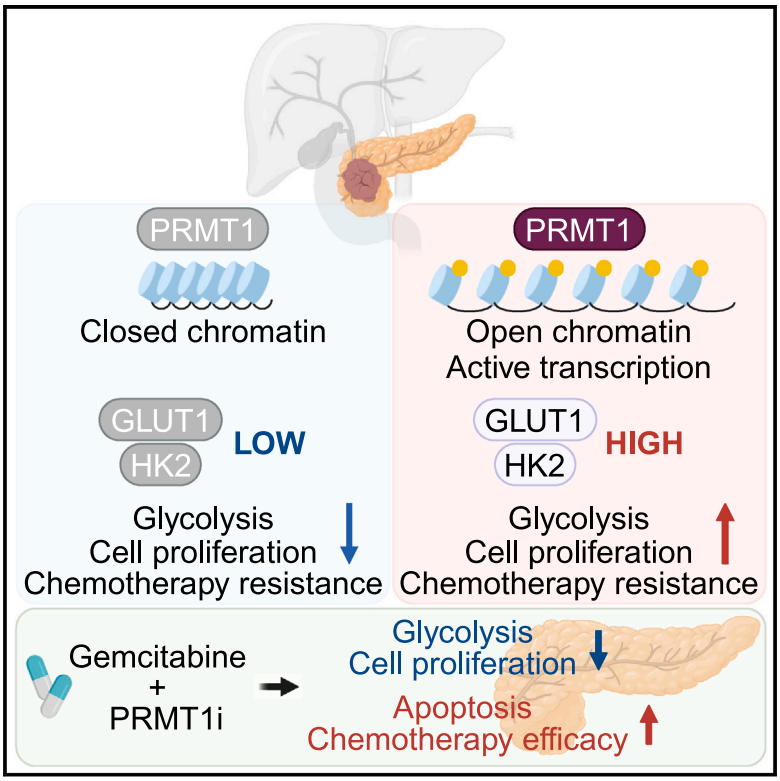

Highlights

- PRMT1 is an early prognostic indicator of PDAC development
- PRMT1 modulates the chromatin landscape in malignant cells
- PRMT1 is an important regulator of glycolysis in PDAC
- Inhibiton of PRMT1 synergizes with gemcitabine treatment

Authors

Bomin Ku, David Eisenbarth, Seonguk Baek, ..., Sang Myung Woo, Sun-Young Kong, Dae-Sik Lim

Correspondence

daesiklim@kaist.ac.kr

In brief

Ku et al. show that PRMT1-mediated changes in chromatin accessibility and transcription control the development and progression of pancreatic cancer by elevating glycolytic activity. Inhibition of PRMT1 in combination with gemcitabine treatment shows favorable results in preclinical models, advocating for further clinical consideration.

Ku et al., 2024, Cell Reports Medicine 5, 101461
March 19, 2024
https://doi.org/10.1016/j.xcrm.2024.101461

CellPress

Cell Reports Medicine

CellPress
OPEN ACCESS

Article

PRMT1 promotes pancreatic cancer development and resistance to chemotherapy

Bomin Ku,[1,7] David Eisenbarth,[1,2,7] Seonguk Baek,[1] Tae-Keun Jeong,[1] Ju-Gyeong Kang,[1] Daehee Hwang,[1] Myung-Giun Noh,[3] Chan Choi,[3] Sungwoo Choi,[1] Taejun Seol,[1] Hail Kim,[4] Yun-Hee Kim,[5] Sang Myung Woo,[5] Sun-Young Kong,[6] and Dae-Sik Lim[1,8,*]

[1]National Creative Research Center for Cell Plasticity, KAIST Stem Cell Center, Department of Biological Sciences, KAIST, Daejeon 34141, Republic of Korea

[2]Brown Center for Immunotherapy, Department of Medicine, Indiana University School of Medicine, Indianapolis, IN 46202, USA

[3]Department of Pathology, Chonnam National University Medical School and Hwasun Hospital, Hwasun-gun, Jeonnam 58128, Republic of Korea

[4]Graduate School of Medical Science and Engineering, Korea Advanced Institute of Science and Technology, Daejeon 34141, Republic of Korea

[5]Research Institute, National Cancer Center, Goyang 10408, Republic of Korea

[6]Targeted Therapy Branch, Division of Rare and Refractory Cancer, Research Institute, National Cancer Center, Goyang 10408, Republic of Korea

[7]These authors contributed equally

[8]Lead contact

*Correspondence: daesiklim@kaist.ac.kr

https://doi.org/10.1016/j.xcrm.2024.101461

SUMMARY

Pancreatic ductal adenocarcinoma (PDAC) remains one of the most lethal types of cancer, and novel treatment regimens are direly needed. Epigenetic regulation contributes to the development of various cancer types, but its role in the development of and potential as a therapeutic target for PDAC remains underexplored. Here, we show that PRMT1 is highly expressed in murine and human pancreatic cancer and is essential for cancer cell proliferation and tumorigenesis. Deletion of PRMT1 delays pancreatic cancer development in a KRAS-dependent mouse model, and multi-omics analyses reveal that PRMT1 depletion leads to global changes in chromatin accessibility and transcription, resulting in reduced glycolysis and a decrease in tumorigenic capacity. Pharmacological inhibition of PRMT1 in combination with gemcitabine has a synergistic effect on pancreatic tumor growth *in vitro* and *in vivo*. Collectively, our findings implicate PRMT1 as a key regulator of pancreatic cancer development and a promising target for combination therapy.

INTRODUCTION

Pancreatic cancer is one of the most lethal types of cancer, boasting the lowest 5-year survival rate among the most frequently diagnosed types.[1] Pancreatic ductal adenocarcinoma (PDAC) is the most common malignancy of the pancreas,[2] and oncogenic mutations of *KRAS* (Kirsten rat sarcoma viral oncogene homolog) are present in more than 80% of patients.[3] Despite extensive efforts, there has been no substantial improvement in the prognosis of individuals diagnosed with PDAC in many years. The main reasons that the outlook for PDAC remains dismal are the lack of reliable predictive indicators for early diagnosis and the limited availability of therapeutic options.[4]

Recent advances in high-throughput sequencing technologies have opened up new possibilities for the study of epigenetic mechanisms in disease development and progression.[5] Epigenetic changes have since been implicated in the pathogenesis of PDAC, and mutations in epigenetic regulators, such as histone-modifying enzymes and the SWI/SNF chromatin remodeling complex, are frequently observed.[6,7] Mutations in these genes can induce neoplastic proliferation through global epigenetic changes and epigenetic inactivation of tumor suppressor genes.[8] One of the most prevalent post-translational modifications (PTMs) is arginine methylation, which is catalyzed by protein arginine methyl transferases (PRMTs) via the transfer of methyl groups from S-adenosyl methionine.[9] Members of the PRMT family of proteins are categorized into three subtypes based on their final methylation product. Although all PRMTs generate monomethyl arginine, only type 1 and 2 PRMTs catalyze the transfer of an additional methyl residue. Type 1 PRMTs generate asymmetric di-methyl arginine (ADMA), whereas type 2 PRMTs produce symmetric di-methyl arginine. PRMT1 is the predominant type 1 PRMT and is responsible for over 85% of ADMA in mammals.[10] Whereas PRMT1 is able to methylate various protein substrates, its primary methylation target is histone H4.[11] Arginine di-methylation of histone H4 (H4R3me2a) promotes histone acetylation, chromatin accessibility, and transcriptional activation.[12–14] Recent studies have highlighted the

importance of arginine methylation in human disease, with high PRMT1 levels correlating with poor prognosis in many types of cancer.[15–17] Importantly, such studies also corroborate the importance of PRMT1 in the development of pancreatic cancer; however, how PRMT1 contributes to PDAC development and progression is not fully understood, and its relevance to KRAS, the major oncogenic driver of PDAC, or its possibility as a therapeutic target is unexplored.[18,19]

Cancer cells have increased metabolic requirements, and reprogramming of the energy metabolism, particularly glucose metabolism, is a hallmark of cancer.[20] In pancreatic cancer, mutant *KRAS* increases glycolysis through upregulation of the expression of key proteins, such as *SLC2A1* (GLUT1) and *Hexokinase2* (HK2).[21,22] Moreover, elevated glycolysis contributes to the development of resistance to gemcitabine (Gem), a first-line therapeutic option for pancreatic cancer. Recent studies have demonstrated the association between high expression levels of glycolytic genes and poor prognosis in pancreatic cancer.[23,24] Gem monotherapy has been the primary chemotherapeutic choice for pancreatic cancer since 1997, and the current guidelines still recommend Gem mono- or combination therapy.[25,26] However, these treatment regimens do not significantly improve 5-year survival rates, and direct therapeutic targeting of mutant KRAS remains difficult.[27] Given the close association between mutant KRAS signaling and metabolic reprogramming, targeting the tumor metabolism constitutes a promising approach for the treatment of KRAS-driven cancers such as PDAC.[28]

Here, we show that high levels of PRMT1 correlate with poor prognosis in both human and mouse pancreatic cancer. Deletion of PRMT1 effectively attenuates tumorigenesis in a mouse model of pancreatic cancer. The activity of PRMT1 is essential for the regulation of chromatin accessibility and the expression of genes critically involved in glycolysis, such as GLUT1 and HK2. Importantly, we demonstrate that the inhibition of PRMT1 blocks oncogenic KRAS-driven glycolysis and that targeting PRMT1 in combination with Gem constitutes a promising therapeutic strategy for pancreatic cancer. Together, our study highlights PRMT1 as a key prognostic marker and an attractive therapeutic target for pancreatic cancer.

RESULTS

PRMT1 is a prognostic marker of PDAC

To explore the expression levels of methyltransferases in pancreatic cancer, we analyzed a single-cell RNA sequencing (scRNA-seq) dataset (GSE129455) of pancreatic tumors from *Kras*$^{+/LSL\text{-}G12D}$;*Trp53*$^{+/LSL\text{-}R172H}$;*Pdx1-Cre* (*KPC*) mice and found that *Prmt1* and *Prmt2* were the most highly expressed methyltransferases within the duct/cancer cell population (Figures S1A and S1B).[29] To further confirm this finding, we analyzed an additional scRNA-seq dataset of a wild-type (WT) pancreas and a pancreatic tumor from a *Kras*$^{+/LSL\text{-}G12D}$;*Trp53*$^{fl/fl}$;*Pdx1-Cre* (*KP*^{f}*C*) mouse (GSE125588).[30] Integration of the WT and *KP*^{f}*C* data and unsupervised clustering revealed 7 distinct clusters distinguished by their respective marker genes (Figures 1A, 1B, and S1C). Among the PRMT family members, *Prmt1*, *Prmt2*, and *Prmt5* were enriched in mutant cells within the duct/cancer cell population, with *Prmt1* exhibiting the most significant increase (Figures 1C and S1D). Since the high expression level of PRMT1 in our analysis, together with findings from previous studies, suggested that PRMT1 may play an important role in the pathogenesis of PDAC, whereas the role of PRMT2 in cancer development remains controversial, we decided to focus on PRMT1 for further study.[31]

We confirmed increased expression of PRMT1 in a *Kras*$^{+/LSL\text{-}G12D}$;*Trp53*$^{fl/fl}$;*Pdx1-CreERT2;tdTomato* (*KP*^{f}*C*^{ER}) PDAC mouse model, which developed tumors within 1–2 months after induction with tamoxifen (Figure S1E).[32] Immunohistochemical (IHC) staining of cytokeratin 19 (CK19) marked all transformed lesions, and Alcian blue staining marked pancreatic intraepithelial neoplasia (PanIN) lesions within the mutant pancreas. Importantly, we observed the increased expression of PRMT1 across all transformed regions, including acinar-to-ductal metaplasia (ADM), PanIN, and PDAC lesions (Figure 1D). To assess whether PRMT1 is also overexpressed in human PDAC, we analyzed expression datasets of human pancreatic adenocarcinoma (PAAD) tumors and adjacent normal tissue from The Cancer Genome Atlas (TCGA) and Genotype-Tissue Expression databases. Consistent with our observations in our mouse model, the expression level of *PRMT1* was significantly higher in tumor tissue than in adjacent normal tissue (Figure 1E). Furthermore, we found that patients with high *PRMT1* expression had a median survival of only 352.6 days, compared to 463.6 days for those with low *PRMT1* expression levels, demonstrating that high *PRMT1* expression is associated with poor prognosis (Figure 1F). To confirm the biological relevance of PRMT1 in pancreatic cancer development, we established organoids from a tumor of a *KP*^{f}*C*^{ER} mouse and treated them with the PRMT1 inhibitor furamidine (FM). FM treatment for 48 h resulted in a significant decrease in cell viability (Figure 1G). It also reduced the extent of structural deformation, a defining feature of cancerous organoids, and led to a significant decrease in cell proliferation (Figure 1H).[33]

Deletion of PRMT1 delays pancreatic cancer development in mice

To further evaluate the biological importance of PRMT1 in pancreatic cancer development *in vivo*, we crossed *KP*^{f}*C*^{ER} mice with *Prmt1*$^{fl/fl}$ mice to generate *Kras*$^{+/LSL\text{-}G12D}$;*Trp53*$^{fl/fl}$;*Prmt1*$^{fl/fl}$;*tdTomato;Pdx1-CreERT2* (*KP*^{f}*C*^{ER};*Prmt1*) mice (Figure 2A). To activate the expression of the Cre recombinase, we intraperitoneally administered tamoxifen on 3 alternate days at 3 to 4 weeks of age (Figure 2B). We confirmed the efficiency of Cre-mediated deletion of *Prmt1* by immunofluorescence (IF) staining of PRMT1 in transformed lesions of the pancreas of *KP*^{f}*C*^{ER};*Prmt1* mice (Figure S2A). Histological analysis of the pancreas revealed that all (7 out of 7) of the *KP*^{f}*C*^{ER} mice developed moderate to poorly differentiated PDAC, whereas only 1 out of 7 (14.3%) *KP*^{f}*C*^{ER};*Prmt1* mice developed well-differentiated PDAC 1 month after tamoxifen administration. Notably, the precancerous lesions in *KP*^{f}*C*^{ER};*Prmt1* mice rarely progressed to PDAC, whereas all of the *KP*^{f}*C*^{ER} mice developed poorly differentiated PDAC as assessed by H&E, Alcian blue, and CK19 staining, suggesting PRMT1 as a key factor in PDAC development and progression (Figures 2C, 2D, and

CellPress
OPEN ACCESS

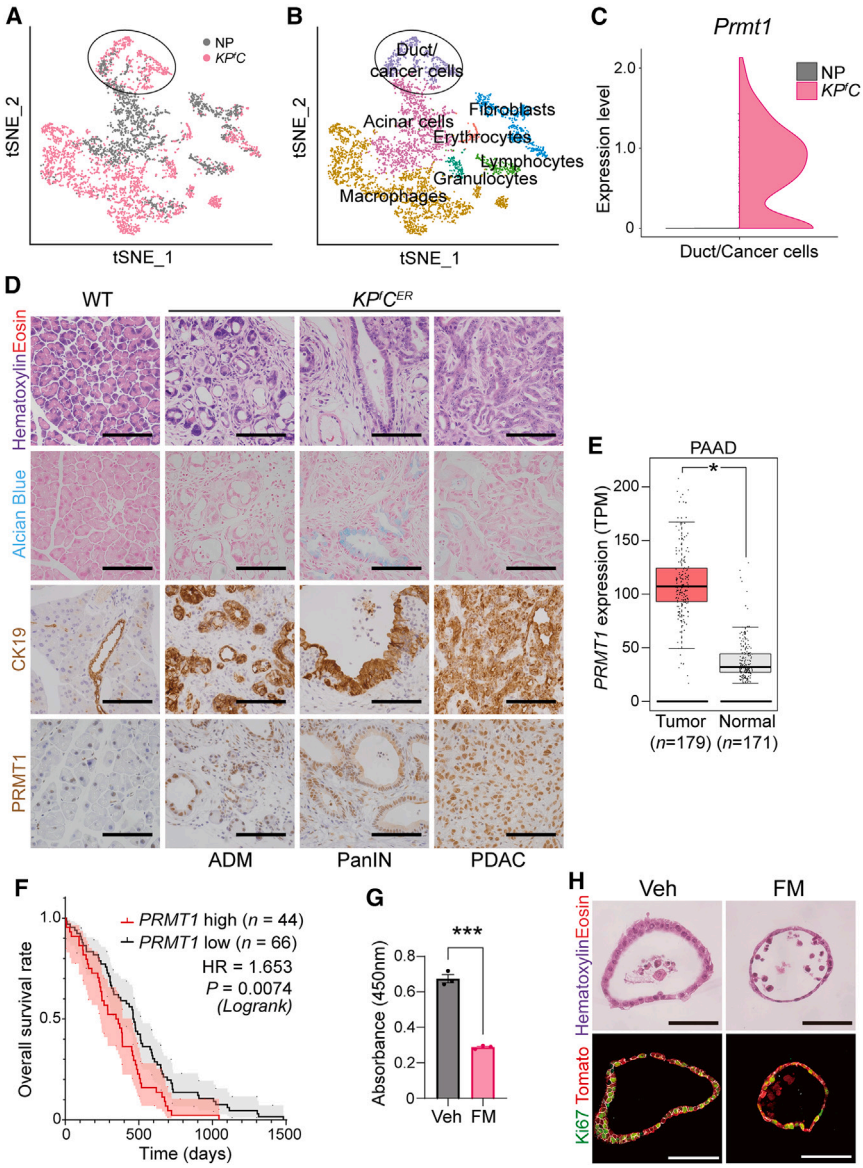

Figure 1. PRMT1 is highly expressed in pancreatic cancer cells

(A) Unsupervised clustering of all viable cells from the pancreas of WT (normal pancreas [NP], gray) and *KP^{f}C* (pink) mice represented as a t-distributed stochastic neighbor embedding plot (GSE125588).

(B) Unsupervised clustering of all viable cells in (A), depicting the indicated cell populations.

(C) Violin plot depicting the expression level of *Prmt1* in the duct/cancer cell population of WT and *KP^{f}C* mice.

(D) Representative H&E staining, Alcian blue staining, and CK19 and PRMT1 IHC staining in the pancreas of WT mice, as well as in ADM, PanIN, and PDAC lesions in the pancreas of *KP^{f}C^{ER}* mice. Scale bars, 100 μm.

(E) Box and whisker plot of *PRMT1* expression in human PAAD tumors (n = 179) and adjacent normal tissue (n = 171). *p < 0.05.

(F) Kaplan-Meier analysis of overall survival in human PAAD patients with high *PRMT1* (n = 44) versus low *PRMT1* (n = 66) expression.

(G) Bar graph showing cell viability in *KP^{f}C^{ER}* mouse pancreatic tumor-derived organoids after treatment with 50 μM FM or Veh for 48 h. n = 3 independent experiments in triplicate. ***p < 0.001.

(H) Representative H&E staining and IF staining for tdTomato and Ki67 in *KP^{f}C^{ER}* organoids (G). Scale bars, 50 μm.

See also Figure S1.

S2B; Table S1). Strikingly, while none of the *KP^{f}C^{ER}* mice survived for more than 87 days after induction, the overall lifespan of *KP^{f}C^{ER};Prmt1* mice more than doubled (Figure 2E). Consistent with our *in vitro* data from inhibitor-treated organoids, transformed lesions in the pancreas of *KP^{f}C^{ER};Prmt1* mice showed a reduced level of cell proliferation (Figures 2F and 2G). Together, these findings demonstrate that the loss of PRMT1 impairs the development and progression of PDAC in mice.

PRMT1 deficiency attenuates glycolysis-related gene expression

We next investigated the molecular mechanism by which the loss of PRMT1 impeded pancreatic cancer development. We depleted *PRMT1* in the 2 human pancreatic cancer cell lines PANC-1 and MiaPaca-2 and confirmed the efficient knockdown and subsequent loss of H4R3me2a by immunoblot (Figure 3A). The loss of PRMT1 resulted in a significant inhibition of cell proliferation and colony formation in both cell lines (Figures 3B and 3C). To evaluate whether pharmacological inhibition of PRMT1 could recapitulate the above observations, we treated MiaPaca-2 and mouse pancreatic cancer-1 (MPC-1) cells, established from the tumor of a *KP^{f}C^{ER}* mouse, with 2 different PRMT1 inhibitors, FM and TC-E 5003 (TCE). We observed reduced histone H4 methylation, cell growth, and colony formation efficiency when cells were treated with these PRMT1 inhibitors (Figures S3A–S3H). Since the chromatin landscape and the transcriptome repertoire may play important roles in the pathological plasticity of pancreatic cancer, we examined whether the depletion of PRMT1 results in significant changes thereof by performing RNA-seq, assay of transposase accessible chromatin (ATAC)-seq, and chromatin immunoprecipitation (ChIP)-seq in control and PRMT1-knockdown MiaPaca-2 cells (Figure 3D).[6] Analysis of our RNA-seq data revealed that the depletion of *PRMT1* resulted in global changes in transcription, with 58.4% of the 858 differentially expressed genes being downregulated and 41.6% being upregulated in PRMT1-depleted cells (Figures 3E and 3F). Pathways most significantly inhibited by the ablation of PRMT1 were related to glycolysis, hypoxia, and mammalian target of rapamycin complex 1 (mTORC1) (Figure 3G). Gene set enrichment analysis (GSEA) further confirmed the

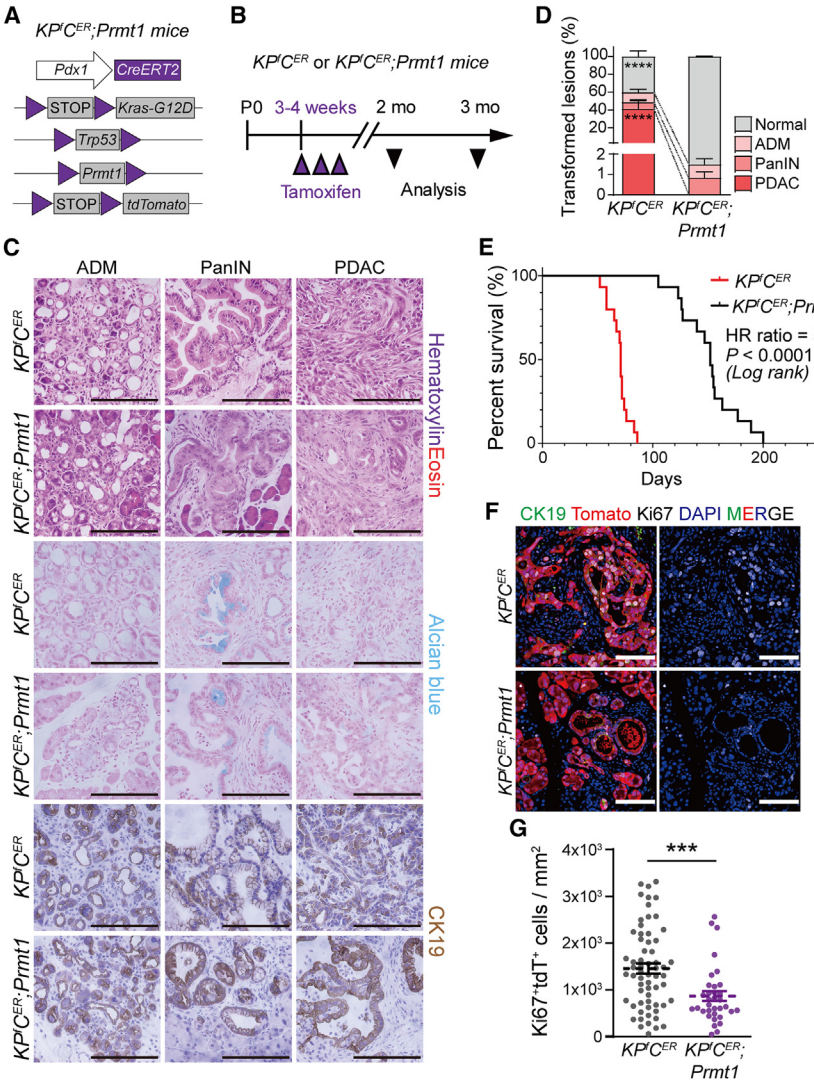

Figure 2. Loss of PRMT1 impairs PDAC development

(A) Genotype of *KP^{f}C^{ER};Prmt1* mice.

(B) Experimental strategy for pancreas-specific genetic modification and analysis of *KP^{f}C^{ER}* and *KP^{f}C^{ER};Prmt1* mice.

(C) Representative H&E staining, Alcian blue staining, and CK19 IHC staining in ADM, PanIN, and PDAC lesions in the pancreas of *KP^{f}C^{ER}* and *KP^{f}C^{ER};Prmt1* mice 2 months after the administration of tamoxifen. Scale bars, 100 μm.

(D) Quantification of transformed lesions in the pancreas of *KP^{f}C^{ER}* and *KP^{f}C^{ER};Prmt1* mice 2 months after the administration of tamoxifen (n = 4 per group). Statistical analyses were performed by two-way ANOVA. ****p < 0.0001

(E) Kaplan-Meier analysis of overall survival for *KP^{f}C^{ER}* (red) and *KP^{f}C^{ER};Prmt1* (black) mice (n = 15 per group). The hazard ratio and p value determined with the log rank test are shown.

(F) Representative IF staining of Ki67, tdTomato, and CK19 in transformed lesions of the pancreas of *KP^{f}C^{ER}* and *KP^{f}C^{ER};Prmt1* mice 2 months after the administration of tamoxifen.

(G) Quantification of Ki67^{+}tdTomato^{+} cells in the pancreas of *KP^{f}C^{ER}* (n = 5) and *KP^{f}C^{ER};Prmt1* (n = 4) mice from images in (F). Data are for a total of 63 and 34 lesions, respectively. Scale bars, 100 μm. ***p < 0.001.

See also Figure S2 and Table S1.

downregulation of glycolytic genes in PRMT1-depleted cells (Figures 3H and 3I; Table S2). Accordingly, several KRAS-induced genes crucial in glycolysis, such as *HK2* and *solute carrier family 2* (*SLC2A1*, also known as *glucose transporter 1*),[21,22] were downregulated in PRMT1-knockdown cells (Figure 3J).

PRMT1 controls the expression of key genes of glycolysis

Given that PRMT1 increases chromatin accessibility and facilitates histone acetylation,[12,13] we performed ATAC-seq in PRMT1 knockdown and shRNA of non-targeting control (shNTC) MiaPaca-2 cells and obtained a total of 52,510 peaks, including 33,345 shared peaks, 13,765 peaks specific to control cells, and 5,400 peaks specific to PRMT1 knockdown samples (Figure 4A). The loss of PRMT1 led to the global adoption of a closed chromatin state (Figure 4B). We then compared ChIP-seq data (GSE29611)[34] obtained for the active chromatin mark H3K27ac and the promoter mark H3K4me3 with our ATAC-seq data. This revealed that open chromatin regions overlapped with peak regions of both active histone marks, and that PRMT1-depleted cells showed reduced chromatin accessibility in both H3K27ac and H3K4me3 peak regions, suggesting that PRMT1-driven chromatin changes can lead to transcriptional changes (Figure 4C). We then annotated these peaks to the nearest transcriptional start site and identified the regions where ATAC signals had been lost following PRMT1 depletion. Next, we defined differentially accessible chromatin regions ($p < 0.05$, 10,822 peak regions) and found that PRMT1 depletion significantly reduced the ATAC-seq peak read density at these regions (Figure 4D). We then filtered these regions with a FC (fold change) <-1.5 to obtain 7,524 PRMT1-dependent open chromatin regions (6,314 unique genes) with reduced mean read density upon PRMT1 depletion. More than half (54.4%) of these regions were located in promoter regions, whereas 40.4% were located in introns or intergenic regions (Figure 4E). In addition, *de novo* motif enrichment analysis for the differentially accessible chromatin regions identified putative binding sites for several transcription factors known to play an important role in the pathogenesis of PDAC, such as CTCF, KLF5, JUNB, CREB, and E2F1, further implying an important role for PRMT1 in the development of PDAC (Figure 4F).[35] To better consolidate the changes in the chromatin landscape and the transcriptional repertoire, we compiled a list of 206 genes that showed both downregulation of expression in our RNA-

CellPress
OPEN ACCESS

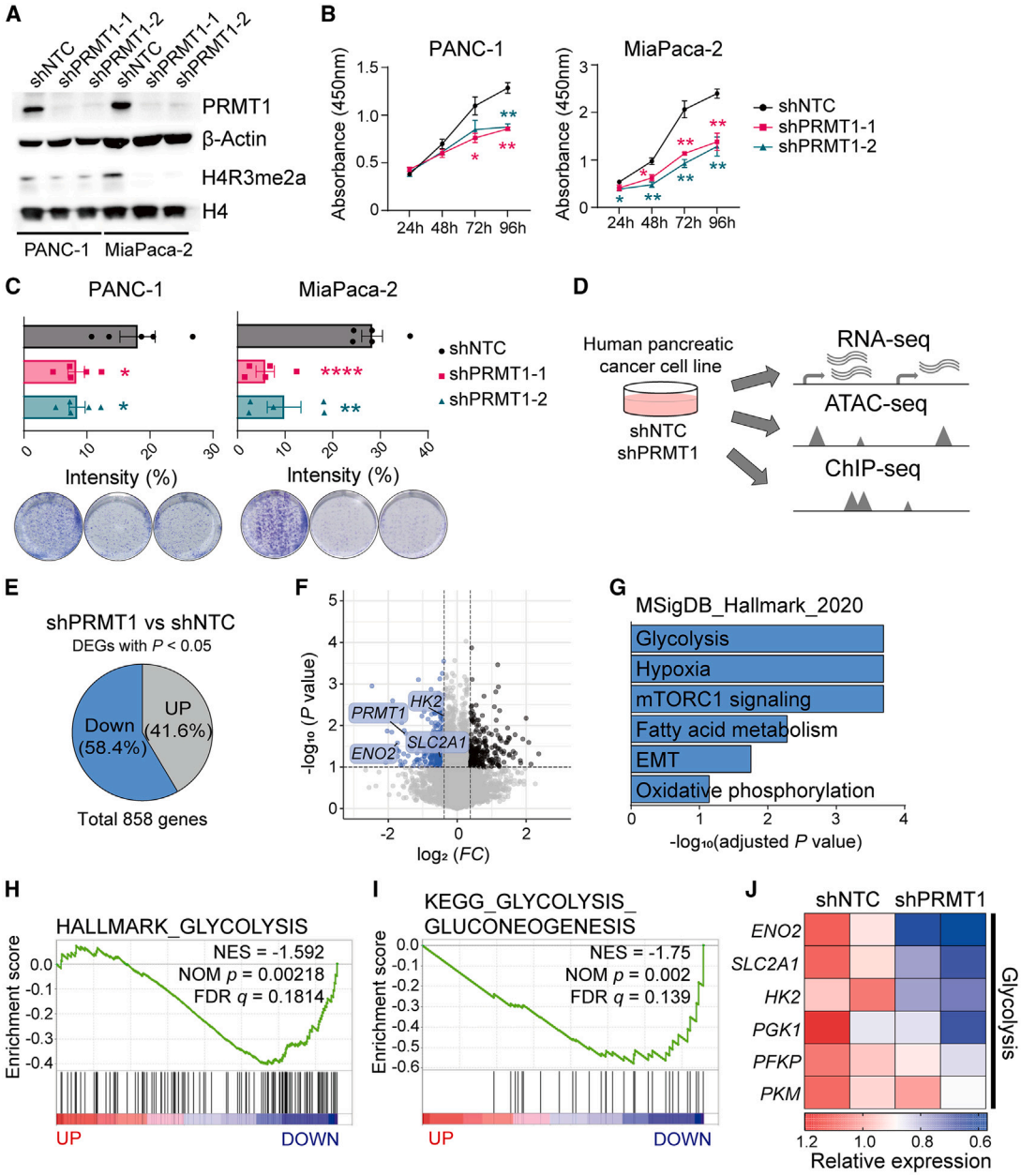

Figure 3. Loss of PRMT1 inhibits glycolysis-related gene expression in PDAC cells

(A) Immunoblot analysis of PRMT1, H4R3me2a, H4, and β-actin (loading control) in PANC-1 and MiaPaca-2 cells infected with lentiviral vectors for 2 independent PRMT1 short hairpin RNAs (shRNAs) or a control shRNA (shNTC). n = 3 independent experiments.

(B) Time course of cell proliferation for cells as in (A). n = 3 independent experiments.

(C) Colony formation assay for cells as in (A), with quantitative data (top) and representative images (bottom) being shown. n = 3 independent experiments.

(D) Schematic representation of the multi-omics analysis.

(E) Pie chart showing the distribution of 858 differentially expressed genes ($p < 0.05$) from the RNA-seq analysis of PRMT1-depleted versus control (shNTC) MiaPaca-2 cells.

(F) Volcano plot showing key downregulated (blue dot), upregulated (black dot), and nonsignificant (gray dot) genes in PRMT1-depleted MiaPaca-2 cells. Vertical line indicates $|\log_2 FC| = 0.3785$ and horizontal line indicates $-\log_{10}$ (p value) = 1. Key downregulated genes are highlighted in blue boxes.

(G) Pathway analysis for genes downregulated by the loss of PRMT1 as in (E).

(H and I) GSEAPreranked enrichment plot showing the enrichment of hallmark glycolysis genes (H) and Kyoto Encyclopedia of Genes and Genomes glycolysis/gluconeogenesis genes (I) in control versus PRMT1-depleted cells. FDR, false discovery rate; NES, normalized enrichment score; NOM *p*, nominal p value.

(J) Heatmap for the expression of selected genes related to glycolysis in control and PRMT1-depleted cells.

*p < 0.05, **p < 0.01, ****p < 0.0001.

See also Figure S3 and Table S2.

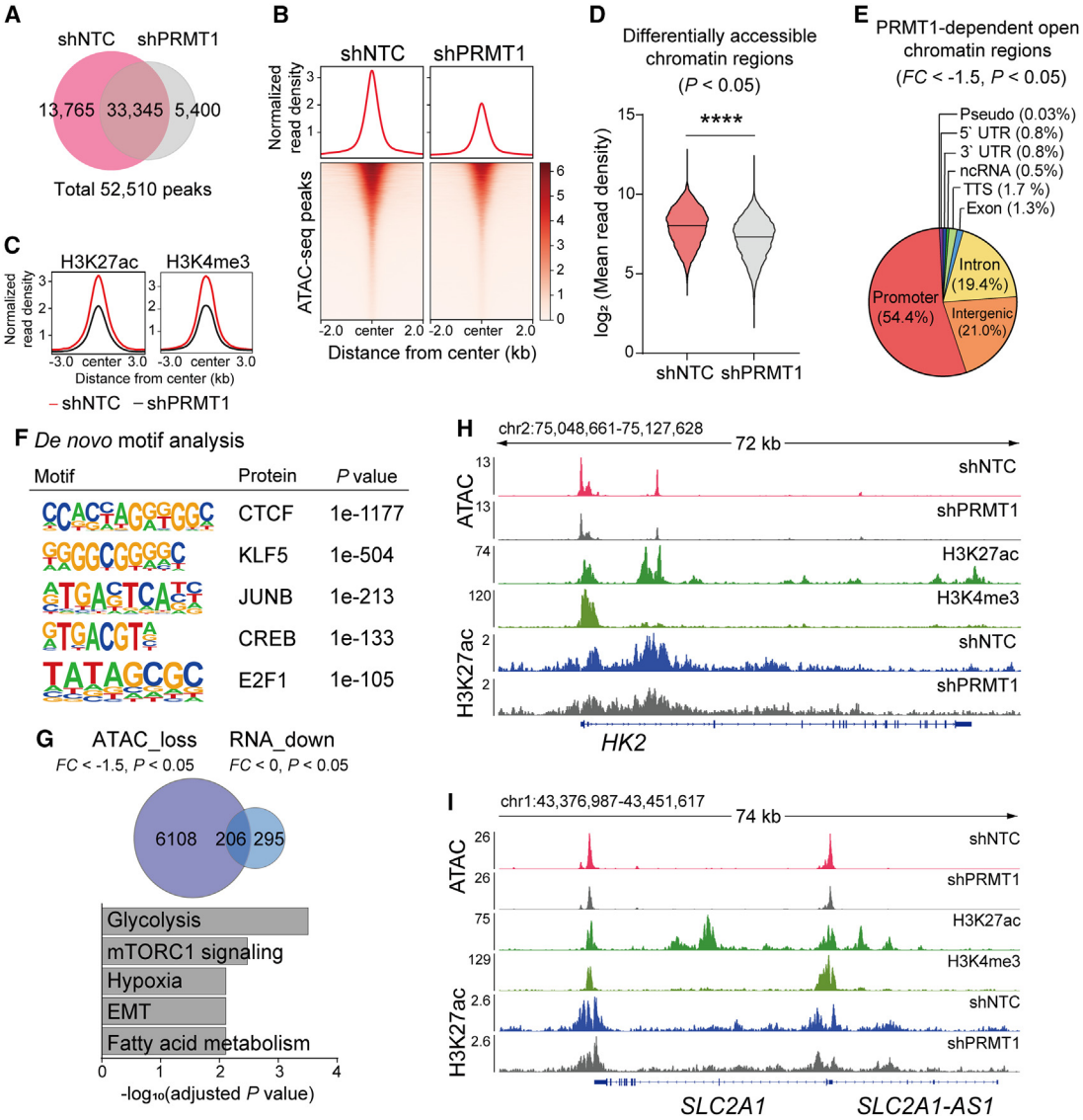

Figure 4. Multi-omics analysis reveals PRMT1-dependent changes in chromatin accessibility

(A) Total number of peaks identified by ATAC-seq analysis of control (shNTC) and PRMT1-knockdown MiaPaca-2 cells.

(B) Heatmap of normalized ATAC-seq intensity and signal distribution histogram around the peak center of ATAC-seq reads in control and PRMT1-depleted cells.

(C) Profile plot of ATAC-seq read density across H3K27ac and H3K4me3 ChIP-seq peak centers.

(D) Violin plot of mean read density of ATAC-seq for differentially accessible chromatin regions ($p < 0.05$). Horizontal lines indicate the median. Statistical analyses were performed by 2-tailed paired Student's t test.****$p < 0.0001$.

(E) Pie chart showing the genomic distribution of PRMT1-dependent open chromatin regions (FC <−1.5, $p < 0.05$).

(F) *De novo* motif analysis of differentially accessible chromatin regions.

(G) Pathway analysis for 206 genes showing both downregulation in RNA-seq experiments and signal loss in ATAC-seq experiments using MSigDB_Hallmark_2020 in response to the depletion of PRMT1.

(H and I) Representative Integrative Genomics Viewer tracks of ATAC-seq and H3K27ac ChIP-seq peaks in control (shNTC) and PRMT1-knockdown MiaPaca-2 cells aligned with H3K27ac and H3K4me3 ChIP-seq peaks (GSE29611) in *HK2* (H) and *SLC2A1* (I).

seq analysis (501 genes) and loss of ATAC-seq signals (6,314 unique genes) in response to PRMT1 depletion. Pathway analysis revealed that glycolysis, mTORC1 signaling, and hypoxia were most strongly affected by the loss of PRMT1 (Figure 4G). Furthermore, we observed that ATAC-seq peaks in the promoter and enhancer regions of the glycolytic genes *HK2* and *SLC2A1* colocalized with H3K27ac and H3K4me3 ChIP-seq signals and showed a reduction in H3K27ac peak signals in response to PRMT1 depletion (Figures 4H and 4I). Together, these data suggest that PRMT1 controls the gene expression of key regulators of glycolysis by inducing more permissive chromatin states in promoter and enhancer regions.

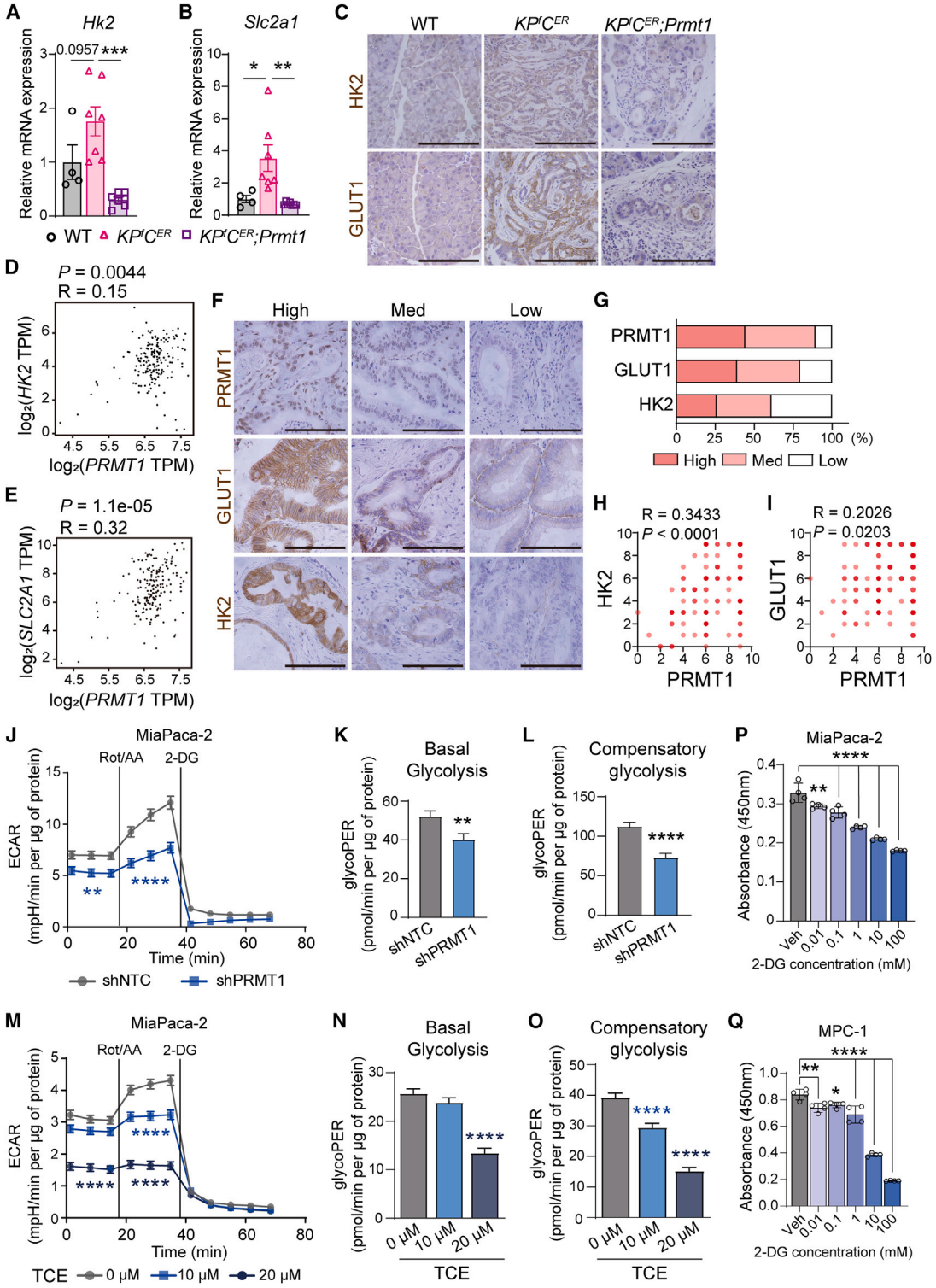

Figure 5. PRMT1 regulates glycolysis in PDAC

(A and B) qRT-PCR analysis of *Hk2* (A) and *Slc2a1* (B) expression in the pancreas of WT (n = 4), KP^fC^{ER} (n = 7), and KP^fC^{ER};*Prmt1* (n = 7) mice.

(C) Representative IHC staining of HK2 and GLUT1 in the pancreas of WT mice and in transformed lesions of the pancreas of KP^fC^{ER} and KP^fC^{ER};*Prmt1* mice. Scale bars, 100 µm.

(D and E) Scatterplots showing positive correlation of *HK2* (D) and *SLC2A1* (E) with *PRMT1* expression in human PAAD patients.

(legend continued on next page)

PRMT1-induced glycolysis contributes to the tumorigenesis of PDAC

To further confirm that glycolysis is enhanced in PDAC cells, we revisited the scRNA-seq data analyzed in Figure 1 and found that the expression of *Hk2* and *Slc2a1* was enriched in the pancreatic duct/cancer cell population of $KP^{f}C$ mice (Figures S4A and S4B). qRT-PCR analysis revealed that the increased expression levels of *Hk2* and *Slc2a1* observed in tumors of $KP^{f}C^{ER}$ mice were attenuated in $KP^{f}C^{ER}$*;Prmt1* mice (Figures 5A and 5B). IHC staining of HK2 and GLUT1 further confirmed reduced levels of glycolysis in the transformed lesions of $KP^{f}C^{ER}$*;Prmt1* mice (Figure 5C). In human PDAC patients, *HK2* and *SLC2A1* were also increased in tumor tissue relative to adjacent normal tissue, and their expression positively correlated with that of *PRMT1* (Figures 5D, 5E, S4C, and S4D). Next, we stained a human tissue microarray (TMA) consisting of 131 PDAC patient specimens for PRMT1, GLUT1, and HK2. We found that more than 89%, 79%, and 61% of the samples showed medium to high staining intensities, respectively, further confirming the elevated expression of these genes in human PDAC (Figures 5F and 5G). In addition, we observed a significant positive correlation of HK2 and GLUT1 with PRMT1 expression in the TMA specimens (Figures 5H and 5I). Together, these results indicate that PRMT1 regulates the expression of key glycolytic proteins in pancreatic cancer.

We next tested whether the reduced expression of glycolytic genes induced by the inhibition of *PRMT1* resulted in metabolic changes. For this purpose, we measured changes in the glycolytic rate and mitochondrial respiration in 2 different human pancreatic cancer cell lines. Measurement of relative acidification and quantification of the glycolytic rate revealed that both basal glycolysis and compensatory glycolysis were reduced in PRMT1-depleted and PRMT1 inhibitor-treated cells in a dose-dependent manner (Figures 5J–5O and S4E–S4J). Similarly, assessment of oxidative phosphorylation measured by the oxygen consumption rate revealed reduced mitochondrial respiration in both PRMT1 knockdown and PRMT1 inhibitor-treated cells (Figures S4K–S4N). We also quantified ATP production in both cell lines and observed that both genetic and pharmacological inhibition of PRMT1 resulted in the reduction of ATP production (Figures S4O–S4R). Lastly, we tested whether the direct inhibition of glycolysis affected pancreatic cancer cell proliferation. Inhibition of glycolysis with 2-deoxy-D-glucose (2-DG) resulted in a significant reduction of cell proliferation in both human and mouse pancreatic cancer cell lines, similar to our previous observation in PRMT1-depleted cells (Figures 5P and 5Q). Collectively, these results demonstrate that the inhibition of PRMT1 blocks pancreatic cancer cell proliferation by suppressing glycolysis.

Pharmacological inhibition of PRMT1 synergizes with Gem treatment

To examine the potential relation between the expression of PRMT1, glycolysis, and clinical outcome, we analyzed scRNA-seq data of human PDAC patient-derived organoids (PDOs) treated with 6 of the most commonly prescribed chemotherapeutics (EGAD00001006448).[36] *PRMT1* was highly expressed across all organoid cell populations but retained differences in expression levels between patients (Figures S5A and S5B). By plotting average *PRMT1* or glycolytic gene expression of each individual organoid cluster against the corresponding response to drug treatment, we found that both *PRMT1* and glycolytic gene expression correlated negatively specifically with sensitivity to Gem (Figures 6A and 6B and S5C–S5L). Gem is commonly prescribed for advanced pancreatic cancer, either alone or in combination with other drugs; however, relapse is common.[26,37] Interestingly, recent studies have shown that increased glycolysis promotes the development of resistance to Gem.[23,24] Given that our results implicate PRMT1 as a crucial regulator of glycolysis, we analyzed the survival data of Gem-treated PAAD patients from TCGA database and found that high expression of *PRMT1*, *HK2*, and *SLC2A1* was associated with poor prognosis (Figures 6C, S6A, and S6B). Since we showed that PRMT1 controls the expression of key glycolytic genes, we postulated that the combination of a PRMT1 inhibitor with Gem could improve therapeutic efficacy. To test this notion, we treated both human and mouse pancreatic cancer cells with FM and Gem and found that such combination therapy resulted in a more pronounced decrease in cell viability than did either drug alone, suggesting a synergistic effect of the 2 agents (Figures S6C and S6D). A combination index (CI) <1 and Loewe synergy score >10 provided further support for such a synergistic effect of Gem and FM

(F) Representative IHC staining of PRMT1, GLUT1, and HK2 in 131 human PDAC tissue samples classified as Low, Med, or High according to the area and intensity of staining. Scale bars, 100 μm.
(G) Quantification of PRMT1, GLUT1, and HK2 immunostainings in (F). PRMT1: High, 44.27%; Med, 45.04%; Low, 10.69%. GLUT1: High, 38.93%; Med, 40.46%; Low, 20.61%. HK2: High, 25.95%; Med, 35.11%; Low, 38.93%.
(H and I) Scatterplots of IHC scores showing a positive correlation of HK2 (H) and GLUT1 (I) expression with PRMT1 expression in 131 human PDAC tissue samples in (F).
(J) Representative profile of the glycolytic rate in control (shNTC) and PRMT1-depleted MiaPaca-2 cells (shPRMT1). Vertical lines indicate the addition of rotenone (Rot), antimycin A (AA), and 2-DG. ECAR, extracellular acidification rate.
(K and L) Basal glycolysis (K) and compensatory glycolysis (L) rates in control (shNTC) and PRMT1-depleted MiaPaca-2 cells from (J). GlycoPER, glycolytic proton efflux rate.
(M) Representative profile of the glycolytic rate in TCE-treated MiaPaca-2 cells.
(N and O) Basal glycolysis (N) and compensatory glycolysis (O) rates in TCE-treated MiaPaca-2 cells from (M).
(P and Q) Cell proliferation assay for MiaPaca-2 (P) and MPC-1 (Q) cells incubated in the presence of the indicated concentrations of 2-DG or vehicle for 48 h. n = 3 independent repeats. *R*, Pearson's correlation coefficient.
*p < 0.05, **p < 0.01, ***p < 0.001, ****p < 0.0001.
Statistical analyses were performed by 1-way ANOVA with Tukey's multiple-comparison test (A and B), 2-way ANOVA with Tukey's multiple-comparison test (J and M), or 1-way ANOVA with Dunnett's multiple-comparison test (P and Q).
See also Figure S4.

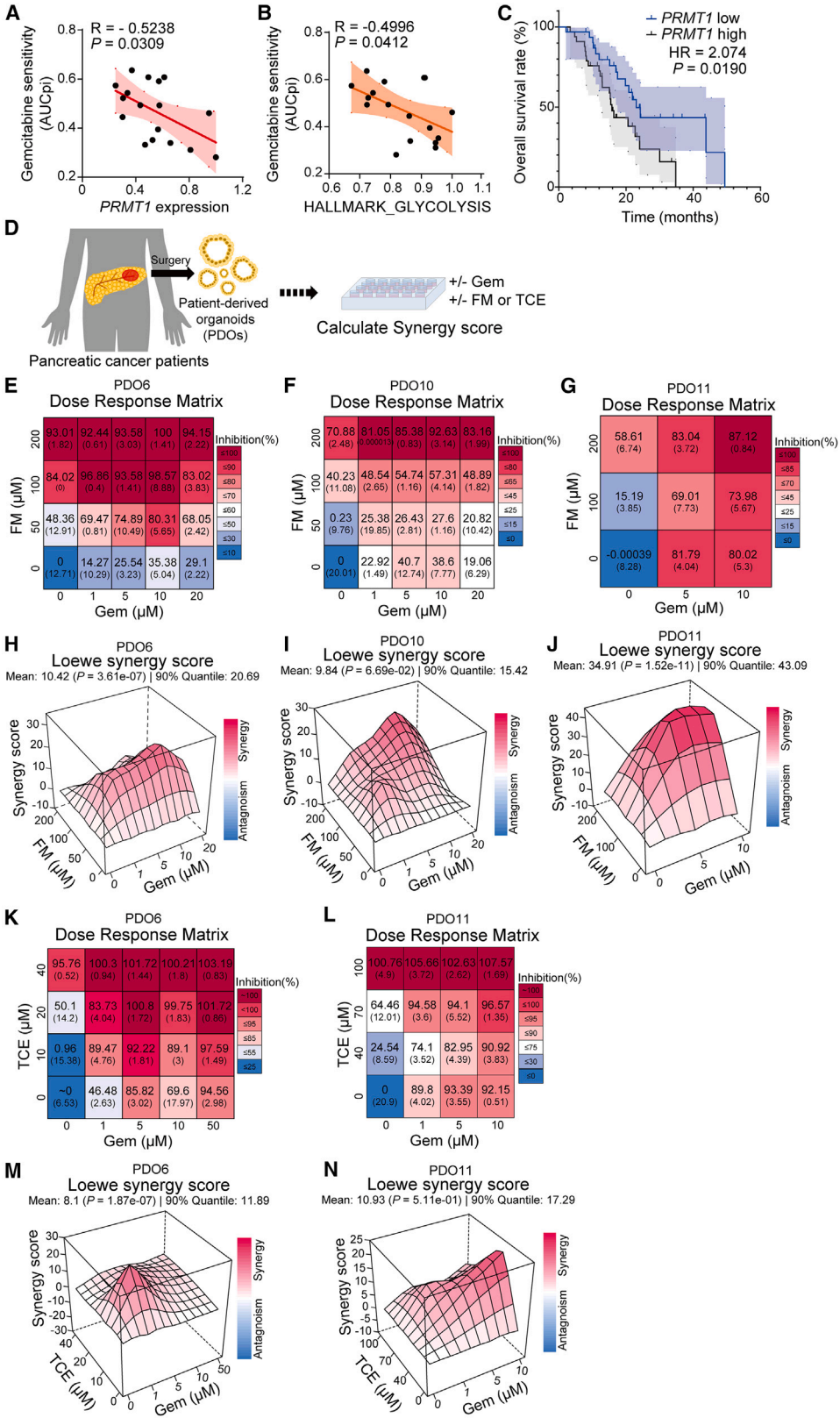

(legend on next page)

(Figures S6E–S6H). Moreover, we observed a similar synergistic effect in cells treated with TCE in combination with Gem (Figures S6I and S6J). To test whether this synergistic effect was also observed in human patients, we treated pancreatic cancer PDOs with multiple doses of each drug (Figure 6D). As observed in cell lines, PDOs treated with both drugs showed reduced cell survival and a synergistic effect of PRMT1 inhibition and Gem (Figures 6E–6N). Our findings demonstrate that the pharmacological inhibition of PRMT1 in pancreatic cancer synergizes with Gem treatment, introducing a promising strategy for treating pancreatic cancer.

PRMT1 inhibition and Gem synergize to suppress PDAC development *in vivo*

To examine the efficacy of this combinatorial therapy *in vivo*, we used a syngeneic allograft model in fully immunocompetent mice by subcutaneous injection of MPC-1 cells. After the tumors had reached a size of ~200 mm^3, we subjected the mice to treatment with either vehicle (Veh), FM only, Gem only, or Gem+FM (Figure 7A). Gem+FM-treated animals showed impaired tumor growth and a markedly reduced tumor volume and weight compared to those treated with either drug alone or vehicle (Figures 7B–7D). IHC staining of HK2 and GLUT1 confirmed reduced glycolytic protein expression in the tumors of Gem+FM-treated animals (Figure 7E). Likewise, tumors isolated from Gem+FM-treated mice also exhibited a decrease in the mRNA expression levels of *Hk2* and *Slc2a1* compared to those isolated from Gem-treated mice (Figures 7F and 7G). Furthermore, we repeated this experiment with TCE and obtained similar results (Figures 7H–7N). To elucidate how PRMT1 inhibition and Gem cooperate to impede tumor growth, we assessed cell proliferation and apoptosis in tumors isolated from these mice. IHC staining of Ki67 and cleaved caspase-3 (cCasp3) confirmed a decrease in cell proliferation and an increase in apoptosis in the tumors treated with Gem+TCE (Figures 7O–7Q). Unfortunately, however, we could not observe tumor regression in these *in vivo* tumor growth experiments. Together, these results suggest that the combination of a PRMT1 inhibitor and Gem constitutes a potent treatment option for pancreatic cancer patients, especially those resistant to Gem.

DISCUSSION

Arginine methylation is one of the most common PTMs and regulates multiple cellular processes, including gene expression, translation, signal transduction, and RNA metabolism.[12,13,19] In this study, we show that PRMT1 induces genome-wide changes in chromatin accessibility and thereby promotes pancreatic cancer development. We demonstrate that PRMT1 controls glycolysis by changing the chromatin landscape and the expression of key glycolytic proteins, which fuels the proliferation and tumorigenic activity of pancreatic cancer cells.

Previous studies have shown the role of PRMT1 in transcriptional regulation and cancer development. For instance, PRMT1-dependent methylation of the proto-oncogene MYC has been implicated in promoting cancer cell proliferation.[38] PRMT1-induced hyperactivation of EGFR and methylation of the transcriptional regulator NONO lead to sustained cell proliferation in colorectal cancer.[39,40] Furthermore, PRMT1-dependent methylation of the histone methyltransferase EZH2 and the transcription factor CEBPA suggests an important role of PRMT1 in the development of breast cancer.[41,42] In hepatocellular carcinoma, cytoplasmic PRMT1 promotes amino acid-induced mTORC1 activation via the methylation of the GATOR2 complex protein WDR24.[43] Interestingly, although most of the studies of PRMT1 in solid tumors show high levels of PRMT1 expression, we and others have observed nuclear localization of PRMT1 in PDAC.[19,44] Given that H4R3me2a leads to the acetylation of adjacent histones and active transcription,[12,14] this study focused on the effect of PRMT1 on histone methylation and the subsequent changes in the chromatin repertoire and transcriptome. Nonetheless, a comprehensive characterization of PRMT1 methylation targets other than histone H4 should further advance our understanding of the role of PRMT1 in the pathogenesis of pancreatic cancer. Peroxisome proliferator-activated receptor gamma coactivator-1α (PGC-1α), for example, is a known PRMT1 methylation target that regulates gene expression related to energy metabolism.[45] Given that PGC-1α regulates mitochondrial biogenesis and the fact that we observed the inhibition of fatty acid metabolism and oxidative phosphorylation, in addition to glycolysis, in PRMT1-depleted cells, suggests that PRMT1 regulates energy metabolism through multiple venues.

A recent study suggested that genotoxic stress-induced PRMT1-dependent methylation of $p14^{ARF}$ plays a tumor-suppressive role in PDAC development.[46] However, primary PDAC has a high inactivation and mutation rate of $p14^{ARF}$, and most pancreatic cancer cell lines, including those used in this study, do not express $p14^{ARF}$.[46] The discrepancy between this study and our observations may be due to the lack of $p14^{ARF}$

Figure 6. Inhibition of PRMT1 synergizes with the therapeutic effect of Gem *ex vivo*

(A and B) Correlation analysis of Gem sensitivity score (AUCpi) and either *PRMT1* expression (A) or the average expression of 200 glycolytic genes (B) in human PDAC organoids. The mean and 95% confidence interval are indicated by the line and shading, respectively. *R*, Pearson's correlation coefficient.

(C) Kaplan-Meier analysis of overall survival for human Gem-treated PAAD patients showing high *PRMT1* (n = 33) versus low *PRMT1* expression (n = 32).

(D) Schematics showing the establishment of PDOs and calculation of the synergy score.

(E–G) Dose-response matrix of the percentage inhibition of cell viability of PDO6 (E), PDO10 (F), and PDO11 (G) in the presence of the indicated drug combinations. Values in each block represent the mean cell viability inhibition with SD.

(H–J) Three-dimensional (3D) plot showing the Loewe synergy score of pairwise dose combinations in PDO6 (H), PDO10 (I), and PDO11 (J). z_axis, synergy score; x/y_axis, Gem+FM combination range.

(K and L) Dose-response matrix of the percentage inhibition of cell viability of PDO6 (K) and PDO11 (L) in the presence of the indicated drug combinations.

(M and N) 3D plot showing the Loewe synergy score of pairwise dose combinations in PDO6 (M) and PDO11 (N). z axis, synergy score; x/y axis, Gem/TCE combination range.

See also Figures S5 and S6.

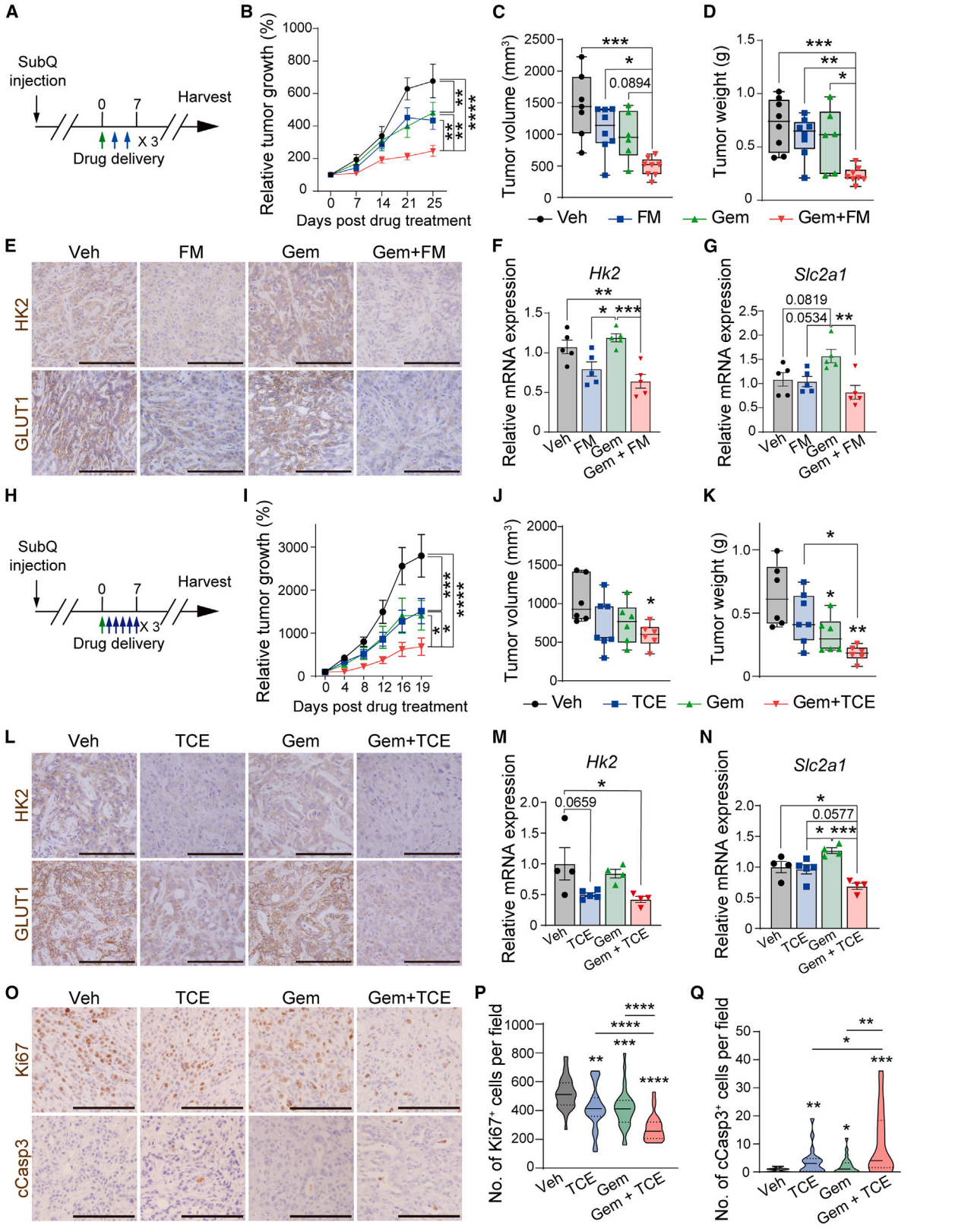

(legend on next page)

expression in most pancreatic cancer cells and the need for genotoxic stress, such as radiation or chemotherapy, to induce PRMT1-dependent methylation of $p14^{ARF}$. Notably, the authors observed a significant increase in the antitumor effect with the combined treatment of the type 1 PRMT inhibitor MS023 and Gem in $p14^{ARF}$-deficient MiaPaca-2 cells, which coincides with our results. Additional studies on the upstream signals that modulate the expression and activity of PRMT1 and its pro- and antitumorigenic downstream targets and their impact on chemoresistance will further help delineate the molecular basis of using PRMT1 as a therapeutic target.

Gem remains one of the most frequently prescribed drugs for pancreatic cancer, but patients quickly develop resistance and relapse is common.[37] Recent studies suggest that elevated levels of glycolysis serve as a potential mechanism to acquire Gem resistance.[23,24] However, most clinical trials of agents targeting metabolic proteins have failed to yield satisfying results, and effective combination treatment strategies remain elusive.[47] We have now shown that the pharmacological inhibition of PRMT1 in combination with Gem treatment significantly attenuated pancreatic cancer cell proliferation *in vitro* and *in vivo*. Collectively, these results suggest that PRMT1 inhibitors are promising candidates for combinatory treatment with Gem, especially in Gem-resistant patients.

Oncogenic mutation of KRAS is present in over 80% of PDAC patients and is the main driver of pancreatic cancer development.[3] We show that *PRMT1* is transcriptionally activated in three separate KRAS-dependent mouse models of PDAC. Oncogenic KRAS induces the transcription of *HK2* and *SLC2A1* in PDAC to answer the need of cancer cells for an increased supply of energy.[21,22] Together with our observation that PRMT1 controls the expression of these genes suggests that PRMT1 may function as a downstream effector of oncogenic KRAS and a signal relay to increase glycolysis. Further studies are warranted to characterize the details of the KRAS-PRMT1-glycolysis signaling axis on the molecular level. Recently, small-molecule inhibitors targeting different mutant KRAS variants have been developed and approved for clinical trials. However, the acquisition of resistance appears to remain a major challenge.[27] It will be interesting to investigate whether PRMT1 inhibition can help overcome resistance to these types of inhibitors. Oncogenic mutation of KRAS is not unique to PDAC, but it is also common in colorectal and lung cancers.[28] In addition, the overexpression of PRMT1 has also been reported in various other types of cancer.[15–17] It will be interesting to see whether KRAS induces the expression of PRMT1 in tissues other than the pancreas, and whether this signaling event plays a role in the tumorigenesis of these types of cancer. Furthermore, Gem is administered for the treatment of a wide range of cancers in addition to PDAC, including bladder, lung, and liver cancers.[48] Our results not only show that the inhibition of PRMT1 potentiates the effect of Gem but also suggest that it may sensitize resistant cancer cells to treatment with Gem. It is thus possible that the benefit of combinatorial treatment with a PRMT1 inhibitor and Gem is not limited to pancreatic cancer.

Together, our work has revealed that PRMT1 controls chromatin accessibility pertaining to the metabolism of cancer cells, and glycolysis in particular. Our findings implicate PRMT1 as an early prognostic marker for pancreatic cancer development and a therapeutic target to overcome Gem resistance.

Limitations of the study

In this study, we focused on PRMT1-mediated regulation of overall chromatin accessibility rather than specific methylation targets of PRMT1, which undoubtedly also play a role in the regulation of glycolysis. Moreover, we performed our experiments exclusively in pancreatic cancer cells. Since we hypothesize that PRMT1 activity is induced by mutant KRAS, other KRAS-driven cancers, such as lung and colorectal cancers, should also show an increase in PRMT1 and subsequent changes in their chromatin landscape and transcription. Especially since Gem is also used in a variety of different cancers, it remains to be explored whether targeting PRMT1 is a valid strategy in a broader context. Despite a clear reduction in tumor growth, we did not observe tumor regression in our *in vivo* experiments. We tested our combination therapy in subcutaneous xenografts, which may not fully recapitulate the natural environment of PDAC. Furthermore, although we evaluated our approach in human cell lines and patient-derived organoids, we did not perform patient-derived xenograft experiments with

Figure 7. Combination of PRMT1 inhibition and Gem impairs pancreatic tumor growth *in vivo*

(A) Schematic representation of subcutaneous implantation and drug administration in mice.
(B) Relative growth curves for tumors of mice from the onset of drug treatment. Veh (n = 8), FM (n = 8), Gem (n = 6), or both (Gem+FM, n = 8).
(C) The volume of tumors isolated from mice after 25 days of drug administration.
(D) Weight of tumors in (C).
(E) Representative IHC staining of HK2 and GLUT1 from tumors in (C). Scale bars, 100 μm.
(F and G) qRT-PCR analysis of *Hk2* (F) or *Slc2a1* (G) mRNA abundance from tumors in (C). n = 5 tumors.
(H) Schematic representation of subcutaneous implantation and drug administration in mice.
(I) Relative growth curves for tumors of mice from the onset of drug treatment. Vehicle (Veh, n = 6), TC-E 5003 (TCE, n = 7), Gem (n = 6), or both (Gem+TCE, n = 6).
(J) The volume of tumors isolated from mice at 19 days of drug administration.
(K) Weight of tumors in (J).
(L) Representative IHC staining of HK2 and GLUT1 from tumors in (J). Scale bars, 100 μm.
(M and N) qRT-PCR analysis of *Hk2* (M) or *Slc2a1* (N) mRNA abundance from tumors in (J). n = 4–5 tumors.
(O) Representative IHC staining of Ki67 and cCasp3 from tumors in (J). Scale bars, 100 μm.
(P and Q) Quantification of Ki67 (P) and cCasp3 (Q) in tumors in (J). (Data are for a total of 37, 26, 32 and 29 lesions, respectively). Horizontal lines indicate the median or quartiles.
*$p < 0.05$, **$p < 0.01$, ***$p < 0.001$, ****$p < 0.0001$.
Statistical analyses were performed by 2-way ANOVA with the Holm-Šídák test (B and I) or 1-way ANOVA with Tukey's multiple-comparison test (C, D, F, G, J, K, M, and N).

human tissues, which may lead to slightly different results. Lastly, the drugs used to block PRMT1 activity still lack specificity and potency, and newly developed inhibitors will hopefully increase the efficacy of this approach.

STAR★METHODS

Detailed methods are provided in the online version of this paper and include the following:

- KEY RESOURCES TABLE
- RESOURCE AVAILABILITY
  - Lead contact
  - Materials availability
  - Data and code availability
- EXPERIMENTAL MODEL AND STUDY PARTICIPANT DETAILS
  - Animal studies
  - Subcutaneous transplantation and drug treatment
  - Cell culture
  - *Ex vivo* mouse and human patient-derived pancreatic tumor organoid culture
  - Tumor microarrays of pancreatic cancer patients
- METHOD DETAILS
  - Histology and IHC staining
  - Immunoblots
  - RNAi
  - Cell proliferation and colony formation assay
  - RNA extraction and quantitative real-time PCR
  - RNA-seq analysis
  - Generation of ATAC-seq samples
  - ChIP-seq library preparation
  - Analysis of ATAC-seq and ChIP-seq data
  - Metabolic analyses
  - Analysis of public datasets
  - Synergy prediction
- QUANTIFICATION AND STATISTICAL ANALYSIS

SUPPLEMENTAL INFORMATION

Supplemental information can be found online at https://doi.org/10.1016/j.xcrm.2024.101461.

ACKNOWLEDGMENTS

This work was supported by grants from the National Research Foundation of Korea (NRF), funded by the Ministry of Science and ICT (MSIT; 2020R1A3B2079551 to D.-S.L. and 2020M3A9A5036362 to S.-Y.K.) and by Brain Pool program funded by the Ministry of Science and ICT through the NRF (RS-2023-00261586 to J.-G.K. and D.-S.L.). We thank Taechang Yang (KAIST) for the preparation of paraffin tissue blocks and H&E staining, Douglas A. Melton (Harvard University) for providing *Pdx1-Cre/ERT2* mice, Christian Conrad (Charité Berlin) for access to the scRNA-seq raw data of PDAC organoids, and the ENCODE project consortium for the generation of datasets. The graphical abstract was created with BioRender.com.

AUTHOR CONTRIBUTIONS

Conceptualization, methodology, validation, data curation, and visualization, B.K. and D.E.; investigation, B.K., D.E., S.B., and T.-K.J.; formal analysis, B.K., D.E., M.-G.N., C.C., and T.S.; resources, H.K., Y.-H.K., and S.M.W.; writing – original draft, B.K. and D.E.; writing – review & editing, B.K., D.E., J.-G.K., D.H., S.C., and D.-S.L.; funding acquisition, J.-G.K., S.-Y.K., and D.-S.L.; supervision, D.-S.L.

DECLARATION OF INTERESTS

The authors declare no competing interests.

Received: February 28, 2023
Revised: December 28, 2023
Accepted: February 14, 2024
Published: March 8, 2024

REFERENCES

1. Siegel, R.L., Miller, K.D., Fuchs, H.E., and Jemal, A. (2022). Cancer statistics, 2022. CA A Cancer J. Clin. *72*, 7–33. https://doi.org/10.3322/caac.21708.
2. Huang, L., Guo, Z., Wang, F., and Fu, L. (2021). KRAS mutation: from undruggable to druggable in cancer. Signal Transduct. Targeted Ther. *6*, 386–420. https://doi.org/10.1038/s41392-021-00780-4.
3. Buscail, L., Bournet, B., and Cordelier, P. (2020). Role of oncogenic KRAS in the diagnosis, prognosis and treatment of pancreatic cancer. Nat. Rev. Gastroenterol. Hepatol. *17*, 153–168. https://doi.org/10.1038/s41575-019-0245-4.
4. Perkhofer, L., Gout, J., Roger, E., Kude De Almeida, F., Baptista Simões, C., Wiesmüller, L., Seufferlein, T., and Kleger, A. (2021). DNA damage repair as a target in pancreatic cancer: State-of-the-art and future perspectives. Gut *70*, 606–617. https://doi.org/10.1136/gutjnl-2019-319984.
5. Feinberg, A.P. (2018). The Key Role of Epigenetics in Human Disease Prevention and Mitigation. N. Engl. J. Med. *378*, 1323–1334. https://doi.org/10.1056/NEJMra1402513.
6. Burdziak, C., Alonso-Curbelo, D., Walle, T., Reyes, J., Barriga, F.M., Haviv, D., Xie, Y., Zhao, Z., Zhao, C.J., Chen, H.A., et al. (2023). Epigenetic plasticity cooperates with cell-cell interactions to direct pancreatic tumorigenesis. Science *380*, eadd5327. https://doi.org/10.1126/science.add5327.
7. Bailey, P., Chang, D.K., Nones, K., Johns, A.L., Patch, A.M., Gingras, M.C., Miller, D.K., Christ, A.N., Bruxner, T.J.C., Quinn, M.C., et al. (2016). Genomic analyses identify molecular subtypes of pancreatic cancer. Nature *531*, 47–52. https://doi.org/10.1038/nature16965.
8. Ougolkov, A.V., Bilim, V.N., and Billadeau, D.D. (2008). Regulation of pancreatic tumor cell proliferation and chemoresistance by the histone methyltransferase enhancer of zeste homologue 2. Clin. Cancer Res. *14*, 6790–6796. https://doi.org/10.1158/1078-0432.CCR-08-1013.
9. Larsen, S.C., Sylvestersen, K.B., Mund, A., Lyon, D., Mullari, M., Madsen, M.V., Daniel, J.A., Jensen, L.J., and Nielsen, M.L. (2016). Proteome-wide analysis of arginine monomethylation reveals widespread occurrence in human cells. Sci. Signal. *9*, rs9-15. https://doi.org/10.1126/scisignal.aaf7329.
10. Tang, J., Frankel, A., Cook, R.J., Kim, S., Paik, W.K., Williams, K.R., Clarke, S., and Herschman, H.R. (2000). PRMT1 is the predominant type I protein arginine methyltransferase in mammalian cells. J. Biol. Chem. *275*, 7723–7730. https://doi.org/10.1074/jbc.275.11.7723.
11. Strahl, B.D., Briggs, S.D., Brame, C.J., Caldwell, J.A., Koh, S.S., Ma, H., Cook, R.G., Shabanowitz, J., Hunt, D.F., Stallcup, M.R., and Allis, C.D. (2001). Methylation of histone H4 at arginine 3 occurs in vivo and is mediated by the nuclear receptor coactivator PRMT1. Curr. Biol. *11*, 996–1000. https://doi.org/10.1016/S0960-9822(01)00294-9.
12. Li, X., Hu, X., Patel, B., Zhou, Z., Liang, S., Ybarra, R., Qiu, Y., Felsenfeld, G., Bungert, J., and Huang, S. (2010). H4R3 methylation facilitates β-globin transcription by regulating histone acetyltransferase binding and H3 acetylation. Blood *115*, 2028–2037. https://doi.org/10.1182/blood-2009-07-236059.

13. Kim, H., Yoon, B.H., Oh, C.M., Lee, J., Lee, K., Song, H., Kim, E., Yi, K., Kim, M.Y., Kim, H., et al. (2020). PRMT1 is required for the maintenance of mature β-cell identity. Diabetes *69*, 355–368. https://doi.org/10.2337/db19-0685.

14. Huang, S., Litt, M., and Felsenfeld, G. (2005). Methylation of histone H4 by arginine methyltransferase PRMT1 is essential in vivo for many subsequent histone modifications. Genes Dev. *19*, 1885–1893. https://doi.org/10.1101/gad.1333905.

15. Gao, Y., Zhao, Y., Zhang, J., Lu, Y., Liu, X., Geng, P., Huang, B., Zhang, Y., and Lu, J. (2016). The dual function of PRMT1 in modulating epithelial-mesenchymal transition and cellular senescence in breast cancer cells through regulation of ZEB1. Sci. Rep. *6*, 19874–19913. https://doi.org/10.1038/srep19874.

16. Zhao, Y., Lu, Q., Li, C., Wang, X., Jiang, L., Huang, L., Wang, C., and Chen, H. (2019). PRMT1 regulates the tumour-initiating properties of esophageal squamous cell carcinoma through histone H4 arginine methylation coupled with transcriptional activation. Cell Death Dis. *10*, 359. https://doi.org/10.1038/s41419-019-1595-0.

17. Mathioudaki, K., Papadokostopoulou, A., Scorilas, A., Xynopoulos, D., Agnanti, N., and Talieri, M. (2008). The PRMT1 gene expression pattern in colon cancer. Br. J. Cancer *99*, 2094–2099. https://doi.org/10.1038/sj.bjc.6604807.

18. Wang, Y., Hsu, J.M., Kang, Y., Wei, Y., Lee, P.C., Chang, S.J., Hsu, Y.H., Hsu, J.L., Wang, H.L., Chang, W.C., et al. (2016). Oncogenic functions of Gli1 in pancreatic adenocarcinoma are supported by its PRMT1-mediated methylation. Cancer Res. *76*, 7049–7058. https://doi.org/10.1158/0008-5472.CAN-16-0715.

19. Giuliani, V., Miller, M.A., Liu, C.-Y., Hartono, S.R., Class, C.A., Bristow, C.A., Suzuki, E., Sanz, L.A., Gao, G., Gay, J.P., et al. (2021). PRMT1-dependent regulation of RNA metabolism and DNA damage response sustains pancreatic ductal adenocarcinoma. Nat. Commun. *12*, 4626. https://doi.org/10.1038/s41467-021-24798-y.

20. Hanahan, D., and Weinberg, R.A. (2011). Hallmarks of cancer: The next generation. Cell *144*, 646–674. https://doi.org/10.1016/j.cell.2011.02.013.

21. Ying, H., Kimmelman, A.C., Lyssiotis, C.A., Hua, S., Chu, G.C., Fletcher-Sananikone, E., Locasale, J.W., Son, J., Zhang, H., Coloff, J.L., et al. (2012). Oncogenic kras maintains pancreatic tumors through regulation of anabolic glucose metabolism. Cell *149*, 656–670. https://doi.org/10.1016/j.cell.2012.01.058.

22. Gaglio, D., Metallo, C.M., Gameiro, P.A., Hiller, K., Danna, L.S., Balestrieri, C., Alberghina, L., Stephanopoulos, G., and Chiaradonna, F. (2011). Oncogenic K-Ras decouples glucose and glutamine metabolism to support cancer cell growth. Mol. Syst. Biol. *7*, 523–615. https://doi.org/10.1038/msb.2011.56.

23. Shukla, S.K., Purohit, V., Mehla, K., Gunda, V., Chaika, N.V., Vernucci, E., King, R.J., Abrego, J., Goode, G.D., Dasgupta, A., et al. (2017). MUC1 and HIF-1alpha Signaling Crosstalk Induces Anabolic Glucose Metabolism to Impart Gemcitabine Resistance to Pancreatic Cancer. Cancer Cell *32*, 71–87.e7. https://doi.org/10.1016/j.ccell.2017.06.004.

24. Xu, F., Huang, M., Chen, Q., Niu, Y., Hu, Y., Hu, P., Chen, D., He, C., Huang, K., Zeng, Z., et al. (2021). LncRNA HIF1A-AS1 promotes gemcitabine resistance of pancreatic cancer by enhancing glycolysis through modulating the AKT/YB1/HIF1a pathway. Cancer Res. *81*, 5678–5691. https://doi.org/10.1158/0008-5472.CAN-21-0281.

25. Wang, S., Zheng, Y., Yang, F., Zhu, L., Zhu, X.Q., Wang, Z.F., Wu, X.L., Zhou, C.H., Yan, J.Y., Hu, B.Y., et al. (2021). The molecular biology of pancreatic adenocarcinoma: translational challenges and clinical perspectives. Signal Transduct. Targeted Ther. *6*, 249. https://doi.org/10.1038/s41392-021-00659-4.

26. Von Hoff, D.D., Ervin, T., Arena, F.P., Chiorean, E.G., Infante, J., Moore, M., Seay, T., Tjulandin, S.A., Ma, W.W., Saleh, M.N., et al. (2013). Increased Survival in Pancreatic Cancer with nab-Paclitaxel plus Gemcitabine. N. Engl. J. Med. *369*, 1691–1703. https://doi.org/10.1056/nejmoa1304369.

27. Awad, M.M., Liu, S., Rybkin, I.I., Arbour, K.C., Dilly, J., Zhu, V.W., Johnson, M.L., Heist, R.S., Patil, T., Riely, G.J., et al. (2021). Acquired Resistance to KRAS G12C Inhibition in Cancer. N. Engl. J. Med. *384*, 2382–2393. https://doi.org/10.1056/nejmoa2105281.

28. Kerk, S.A., Papagiannakopoulos, T., Shah, Y.M., and Lyssiotis, C.A. (2021). Metabolic networks in mutant KRAS-driven tumours: tissue specificities and the microenvironment. Nat. Rev. Cancer *21*, 510–525. https://doi.org/10.1038/s41568-021-00375-9.

29. Elyada, E., Bolisetty, M., Laise, P., Flynn, W.F., Courtois, E.T., Burkhart, R.A., Teinor, J.A., Belleau, P., Biffi, G., Lucito, M.S., et al. (2019). Cross-species single-cell analysis of pancreatic ductal adenocarcinoma reveals antigen-presenting cancer-associated fibroblasts. Cancer Discov. *9*, 1102–1123. https://doi.org/10.1158/2159-8290.CD-19-0094.

30. Hosein, A.N., Huang, H., Wang, Z., Parmar, K., Du, W., Huang, J., Maitra, A., Olson, E., Verma, U., and Brekken, R.A. (2019). Cellular heterogeneity during mouse pancreatic ductal adenocarcinoma progression at single-cell resolution. JCI Insight *5*, e129212–e129216. https://doi.org/10.1172/jci.insight.129212.

31. Hwang, J.W., Cho, Y., Bae, G.U., Kim, S.N., and Kim, Y.K. (2021). Protein arginine methyltransferases: promising targets for cancer therapy. Exp. Mol. Med. *53*, 788–808. https://doi.org/10.1038/s12276-021-00613-y.

32. Park, J., Eisenbarth, D., Choi, W., Kim, H., Choi, C., Lee, D., and Lim, D.S. (2020). YAP and AP-1 cooperate to initiate pancreatic cancer development from ductal cells in Mice. Cancer Res. *80*, 4768–4779. https://doi.org/10.1158/0008-5472.CAN-20-0907.

33. Seino, T., Kawasaki, S., Shimokawa, M., Tamagawa, H., Toshimitsu, K., Fujii, M., Ohta, Y., Matano, M., Nanki, K., Kawasaki, K., et al. (2018). Human Pancreatic Tumor Organoids Reveal Loss of Stem Cell Niche Factor Dependence during Disease Progression. Cell Stem Cell *22*, 454–467.e6. https://doi.org/10.1016/j.stem.2017.12.009.

34. ENCODE Project Consortium; Kundaje, A., Aldred, S.F., Collins, P.J., Davis, C.A., Doyle, F., Epstein, C.B., Frietze, S., Harrow, J., Kaul, R., et al. (2012). An integrated encyclopedia of DNA elements in the human genome. Nature *489*, 57–74. https://doi.org/10.1038/nature11247.

35. Li, Y., He, Y., Peng, J., Su, Z., Li, Z., Zhang, B., Ma, J., Zhuo, M., Zou, D., Liu, X., et al. (2021). Mutant Kras Co-opts a Proto-Oncogenic Enhancer Network in Inflammation-Induced Metaplastic Progenitor Cells to Initiate Pancreatic Cancer. Nature Cancer *2*, 49–65. https://doi.org/10.1038/s43018-020-00134-z.

36. Krieger, T.G., Le Blanc, S., Jabs, J., Ten, F.W., Ishaque, N., Jechow, K., Debnath, O., Leonhardt, C.S., Giri, A., Eils, R., et al. (2021). Single-cell analysis of patient-derived PDAC organoids reveals cell state heterogeneity and a conserved developmental hierarchy. Nat. Commun. *12*, 5826. https://doi.org/10.1038/s41467-021-26059-4.

37. Kim, M.P., and Gallick, G.E. (2008). Gemcitabine resistance in pancreatic cancer: Picking the key players. Clin. Cancer Res. *14*, 1284–1285. https://doi.org/10.1158/1078-0432.CCR-07-2247.

38. Favia, A., Salvatori, L., Nanni, S., Iwamoto-Stohl, L.K., Valente, S., Mai, A., Scagnoli, F., Fontanella, R.A., Totta, P., Nasi, S., and Illi, B. (2019). The Protein Arginine Methyltransferases 1 and 5 affect Myc properties in glioblastoma stem cells. Sci. Rep. *9*, 15925–16013. https://doi.org/10.1038/s41598-019-52291-6.

39. Liao, H.W., Hsu, J.M., Xia, W., Wang, H.L., Wang, Y.N., Chang, W.C., Arold, S.T., Chou, C.K., Tsou, P.H., Yamaguchi, H., et al. (2015). PRMT1-mediated methylation of the EGF receptor regulates signaling and cetuximab response. J. Clin. Invest. *125*, 4529–4543. https://doi.org/10.1172/JCI82826.

40. Yin, X.K., Wang, Y.L., Wang, F., Feng, W.X., Bai, S.M., Zhao, W.W., Feng, L.L., Wei, M.B., Qin, C.L., Wang, F., et al. (2021). PRMT1 enhances oncogenic arginine methylation of NONO in colorectal cancer. Oncogene *40*, 1375–1389. https://doi.org/10.1038/s41388-020-01617-0.

41. Li, Z., Wang, D., Chen, X., Wang, W., Wang, P., Hou, P., Li, M., Chu, S., Qiao, S., Zheng, J., and Bai, J. (2021). PRMT1-mediated EZH2 methylation

promotes breast cancer cell proliferation and tumorigenesis. Cell Death Dis. *12*, 1080–1111. https://doi.org/10.1038/s41419-021-04381-5.

42. Liu, L.M., Sun, W.Z., Fan, X.Z., Xu, Y.L., Cheng, M.B., and Zhang, Y. (2019). Methylation of C/EBPa by PRMT1 inhibits its tumor-suppressive function in breast cancer. Cancer Res. *79*, 2865–2877. https://doi.org/10.1158/0008-5472.CAN-18-3211.

43. Yin, S., Liu, L., Ball, L.E., Wang, Y., Bedford, M.T., Duncan, S.A., Wang, H., and Gan, W. (2023). CDK5-PRMT1-WDR24 signaling cascade promotes mTORC1 signaling and tumor growth. Cell Rep. *42*, 112316. https://doi.org/10.1016/j.celrep.2023.112316.

44. Song, C., Chen, T., He, L., Ma, N., Li, J.A., Rong, Y.F., Fang, Y., Liu, M., Xie, D., and Lou, W. (2020). PRMT1 promotes pancreatic cancer growth and predicts poor prognosis. Cell. Oncol. *43*, 51–62. https://doi.org/10.1007/s13402-019-00435-1.

45. Teyssier, C., Ma, H., Emter, R., Kralli, A., and Stallcup, M.R. (2005). Activation of nuclear receptor coactivator PGC-1α by arginine methylation. Genes Dev. *19*, 1466–1473. https://doi.org/10.1101/gad.1295005.

46. Repenning, A., Happel, D., Bouchard, C., Meixner, M., Verel-Yilmaz, Y., Raifer, H., Holembowski, L., Krause, E., Kremmer, E., Feederle, R., et al. (2021). PRMT1 promotes the tumor suppressor function of p14 ARF and is indicative for pancreatic cancer prognosis. EMBO J. *40*, 1067777–e106821. https://doi.org/10.15252/embj.2020106777.

47. Qin, C., Yang, G., Yang, J., Ren, B., Wang, H., Chen, G., Zhao, F., You, L., Wang, W., and Zhao, Y. (2020). Metabolism of pancreatic cancer: Paving the way to better anticancer strategies. Mol. Cancer *19*, 50–19. https://doi.org/10.1186/s12943-020-01169-7.

48. Toschi, L., Finocchiaro, G., Bartolini, S., Gioia, V., and Cappuzzo, F. (2005). DRUG EVALUATION Role of gemcitabine in cancer therapy. Future Oncol. *1*, 7–17.

49. Jackson, E.L., Willis, N., Mercer, K., Bronson, R.T., Crowley, D., Montoya, R., Jacks, T., and Tuveson, D.A. (2001). Analysis of lung tumor initiation and progression using conditional expression of oncogenic K-ras. Genes Dev. *15*, 3243–3248. https://doi.org/10.1101/gad.943001.

50. Marino, S., Vooijs, M., Van Der Gulden, H., Jonkers, J., and Berns, A. (2000). Induction of medulloblastomas in p53-null mutant mice by somatic inactivation of Rb in the external granular layer cells of the cerebellum. Genes Dev. *14*, 994–1004. https://doi.org/10.1101/gad.14.8.994.

51. Madisen, L., Zwingman, T.A., Sunkin, S.M., Oh, S.W., Zariwala, H.A., Gu, H., Ng, L.L., Palmiter, R.D., Hawrylycz, M.J., Jones, A.R., et al. (2010). A robust and high-throughput Cre reporting and characterization system for the whole mouse brain. Nat. Neurosci. *13*, 133–140. https://doi.org/10.1038/nn.2467.

52. Gu, G., Dubauskaite, J., and Melton, D.A. (2002). Direct evidence for the pancreatic lineage: NGN3+ cells are islet progenitors and are distinct from duct progenitors. Development *129*, 2447–2457. https://doi.org/10.1242/dev.129.10.2447.

53. Choi, W., Kim, Y.-H., Woo, S.M., Yu, Y., Lee, M.R., Lee, W.J., Chun, J.W., Sim, S.H., Chae, H., Shim, H., et al. (2023). Establishment of Patient-Derived Organoids Using Ascitic or Pleural Fluid from Cancer Patients. Cancer Res. Treat. *55*, 1077–1086. https://doi.org/10.4143/crt.2022.1630.

54. Schindelin, J., Arganda-Carreras, I., Frise, E., Kaynig, V., Longair, M., Pietzsch, T., Preibisch, S., Rueden, C., Saalfeld, S., Schmid, B., et al. (2012). Fiji: An open-source platform for biological-image analysis. Nat. Methods *9*, 676–682. https://doi.org/10.1038/nmeth.2019.

55. Guzmán, C., Bagga, M., Kaur, A., Westermarck, J., and Abankwa, D. (2014). ColonyArea: An ImageJ plugin to automatically quantify colony formation in clonogenic assays. PLoS One *9*, 924444–e92517. https://doi.org/10.1371/journal.pone.0092444.

56. Kim, D., Paggi, J.M., Park, C., Bennett, C., and Salzberg, S.L. (2019). Graph-based genome alignment and genotyping with HISAT2 and HISAT-genotype. Nat. Biotechnol. *37*, 907–915. https://doi.org/10.1038/s41587-019-0201-4.

57. Pertea, M., Kim, D., Pertea, G.M., Leek, J.T., and Salzberg, S.L. (2016). Transcript-level expression analysis of RNA-seq experiments with HISAT, StringTie and Ballgown. Nat. Protoc. *11*, 1650–1667. https://doi.org/10.1038/nprot.2016.095.

58. Frazee, A.C., Pertea, G., Jaffe, A.E., Langmead, B., Salzberg, S.L., and Leek, J.T. (2015). Ballgown bridges the gap between transcriptome assembly and expression analysis. Nat. Biotechnol. *33*, 243–246. https://doi.org/10.1038/nbt.3172.

59. Robinson, M.D., McCarthy, D.J., and Smyth, G.K. (2010). edgeR: A Bioconductor package for differential expression analysis of digital gene expression data. Bioinformatics *26*, 139–140. https://doi.org/10.1093/bioinformatics/btp616.

60. Subramanian, A., Tamayo, P., Mootha, V.K., Mukherjee, S., Ebert, B.L., Gillette, M.A., Paulovich, A., Pomeroy, S.L., Golub, T.R., Lander, E.S., and Mesirov, J.P. (2005). Gene set enrichment analysis: A knowledge-based approach for interpreting genome-wide expression profiles. Proc. Natl. Acad. Sci. USA *102*, 15545–15550. https://doi.org/10.1073/pnas.0506580102.

61. Liberzon, A., Birger, C., Thorvaldsdóttir, H., Ghandi, M., Mesirov, J.P., and Tamayo, P. (2015). The Molecular Signatures Database Hallmark Gene Set Collection. Cell Syst. *1*, 417–425. https://doi.org/10.1016/j.cels.2015.12.004.

62. Kanehisa, M., and Goto, S. (2000). KEGG: Kyoto Encyclopedia of Genes and Genomes. Nucleic Acids Res. *28*, 27–30. https://doi.org/10.1093/nar/28.1.27.

63. Chenet al (2013). Enrichr: interactive and collaborative HTML5 gene list enrichment analysis tool. BMC Bioinf. *128*, 1471–2105. https://doi.org/10.1007/s00701-014-2321-4.

64. Kuleshov, M.V., Jones, M.R., Rouillard, A.D., Fernandez, N.F., Duan, Q., Wang, Z., Koplev, S., Jenkins, S.L., Jagodnik, K.M., Lachmann, A., et al. (2016). Enrichr: a comprehensive gene set enrichment analysis web server 2016 update. Nucleic Acids Res. *44*, W90–W97. https://doi.org/10.1093/nar/gkw377.

65. Grandi, F.C., Modi, H., Kampman, L., and Corces, M.R. (2022). Chromatin accessibility profiling by ATAC-seq. Nat. Protoc. *17*, 1518–1552. https://doi.org/10.1038/s41596-022-00692-9.

66. Langmead, B., and Salzberg, S.L. (2012). Fast gapped-read alignment with Bowtie 2. Nat. Methods *9*, 357–359. https://doi.org/10.1038/nmeth.1923.

67. Quinlan, A.R., and Hall, I.M. (2010). BEDTools: A flexible suite of utilities for comparing genomic features. Bioinformatics *26*, 841–842. https://doi.org/10.1093/bioinformatics/btq033.

68. Zhang, Y., Liu, T., Meyer, C.A., Eeckhoute, J., Johnson, D.S., Bernstein, B.E., Nusbaum, C., Myers, R.M., Brown, M., Li, W., and Liu, X.S. (2008). Model-based analysis of ChIP-Seq (MACS). Genome Biol. *9*, R137. https://doi.org/10.1186/gb-2008-9-9-r137.

69. Heinz, S., Benner, C., Spann, N., Bertolino, E., Lin, Y.C., Laslo, P., Cheng, J.X., Murre, C., Singh, H., and Glass, C.K. (2010). Simple Combinations of Lineage-Determining Transcription Factors Prime cis-Regulatory Elements Required for Macrophage and B Cell Identities. Mol. Cell *38*, 576–589. https://doi.org/10.1016/j.molcel.2010.05.004.

70. Ross-Innes, C.S., Stark, R., Teschendorff, A.E., Holmes, K.A., Ali, H.R., Dunning, M.J., Brown, G.D., Gojis, O., Ellis, I.O., Green, A.R., et al. (2012). Differential oestrogen receptor binding is associated with clinical outcome in breast cancer. Nature *481*, 389–393. https://doi.org/10.1038/nature10730.

71. Ramírez, F., Ryan, D.P., Grüning, B., Bhardwaj, V., Kilpert, F., Richter, A.S., Heyne, S., Dündar, F., and Manke, T. (2016). deepTools2: a next generation web server for deep-sequencing data analysis. Nucleic Acids Res. *44*, W160–W165. https://doi.org/10.1093/NAR/GKW257.

72. Robinson, J.T., Thorvaldsdóttir, H., Wenger, A.M., Zehir, A., and Mesirov, J.P. (2017). Variant review with the integrative genomics viewer. Cancer Res. *77*, e31–e34. https://doi.org/10.1158/0008-5472.CAN-17-0337.

73. Hao, Y., Hao, S., Andersen-Nissen, E., Mauck, W.M., Zheng, S., Butler, A., Lee, M.J., Wilk, A.J., Darby, C., Zager, M., et al. (2021). Integrated analysis of multimodal single-cell data. Cell *184*, 3573–3587.e29. https://doi.org/10.1016/j.cell.2021.04.048.

74. Cerami, E., Gao, J., Dogrusoz, U., Gross, B.E., Sumer, S.O., Aksoy, B.A., Jacobsen, A., Byrne, C.J., Heuer, M.L., Larsson, E., et al. (2012). The cBio Cancer Genomics Portal: An open platform for exploring multidimensional cancer genomics data. Cancer Discov. *2*, 401–404. https://doi.org/10.1158/2159-8290.CD-12-0095.

75. Tang, Z., Li, C., Kang, B., Gao, G., Li, C., and Zhang, Z. (2017). GEPIA: A web server for cancer and normal gene expression profiling and interactive analyses. Nucleic Acids Res. *45*, W98–W102. https://doi.org/10.1093/nar/gkx247.

76. Zheng, S., Wang, W., Aldahdooh, J., Malyutina, A., Shadbahr, T., Tanoli, Z., Pessia, A., and Tang, J. (2022). SynergyFinder Plus: Toward Better Interpretation and Annotation of Drug Combination Screening Datasets. Genomics, Proteomics Bioinforma *20*, 587–596. https://doi.org/10.1016/j.gpb.2022.01.004.

77. Chou, T.C. (2010). Drug combination studies and their synergy quantification using the chou-talalay method. Cancer Res. *70*, 440–446. https://doi.org/10.1158/0008-5472.CAN-09-1947.

STAR★METHODS

KEY RESOURCES TABLE

REAGENT or RESOURCE	SOURCE	IDENTIFIER
Antibodies		
PRMT1 antibody	Novus Biologicals	Cat #: NBP2-67074; RRID: AB_3076255
PRMT1 antibody	Sigma-Aldrich	Cat #: 07–404;RRID: AB_310588
Krt19 antibody	DSHB	Cat #: TROMA-III; RRID: AB_2133570
RFP(tdTomato) antibody	Origene	Cat #: AB8181; RRID: AB_2722750
GLUT1 antibody	Millipore	Cat #: 07–1401; RRID: AB_11212210
Hexokinase II antibody	Cell Signaling Technology	Cat #: 2867S; RRID: AB_2232946
β-actin antibody	Sigma-Aldrich	Cat #: A5316; RRID: AB_476743
Vinculin antibody	Cell Signaling Technology	Cat #: 13901S; RRID: AB_2728768
Histone H4 antibody	Abcam	Cat #: ab177840;RRID: AB_2650469
Histone H4R3me2a (asymmetric) antibody	Active Motif	Cat #: 39006; RRID: AB_2793313
Histone H3 (acetyl K27) antibody	Abcam	Cat#: ab4729; RRID: AB_2118291
Ki67 antibody	Abcam	Cat# ab16667; RRID:AB_302459
Cleaved Caspase-3 antibody	Cell Signaling Technology	Cat# 9664S; RRID:AB_2070042
Donkey anti-Rabbit IgG (H + L) Highly Cross-Adsorbed Secondary Antibody, Alexa Fluor™ 488	Invitrogen	Cat #: A-21206; RRID: AB_2535792
Donkey anti-Rat IgG (H + L) Highly Cross-Adsorbed Secondary Antibody, Alexa Fluor™ 488	Invitrogen	Cat #: A-21208; RRID: AB_2535794
Donkey anti-Goat IgG (H + L) Cross-Adsorbed Secondary Antibody, Alexa Fluor™ 594	Invitrogen	Cat #: A-11058; RRID: AB_2534105
Donkey anti-Rabbit IgG (H + L) Highly Cross-Adsorbed Secondary Antibody, Alexa Fluor™ 647	Invitrogen	Cat #: A-31573; RRID: AB_2536183
Donkey anti-Mouse IgG (H + L) Highly Cross-Adsorbed Secondary Antibody, Alexa Fluor™ 647	Invitrogen	Cat #: A-31571; RRID: AB_162542
Biological samples		
Human pancreatic cancer tissue micro array samples	National Biobank of Korea at Chonnam National University Hwasun Hospital	N/A
Human pancreatic cancer patient derived organoids	National Cancer Center, Goyang, South Korea	N/A
Chemicals, peptides, and recombinant proteins		
Gemcitabine	Sigma-Aldrich	Cat #: G6423
Furamidine dihydrochloride	Sigma-Aldrich	Cat #: SML-1559
TC-E 5003	Cayman	Cat #: 17718
B-27™ Supplement	Gibco	Cat #: 17504-04
Nicotinamide	Sigma-Aldrich	Cat #: N0636
Recombinant human FGF10	Peprotech	Cat #: 100-26
N-acetylcysteine	Sigma-Aldrich	Cat #: A9165
Recombinant murine noggin	Peprotech	Cat #: 250-38-100
A83-01	TOCRIS	Cat #: 2939
Human epidermal growth factor	Merck	Cat #: SRP3027
Gastrin	Sigma-Aldrich	Cat #: G9020
Wnt3A conditioned medium	U-protein Express BV	Cat #: N001
Rspondin1	Qkine	Cat #: Qk006
Primocin	Invivogen	Cat #: ant-pm-2
TrypLE Express	Gibco	Cat #: 12604021
ROCKi (Y27632)	Sigma-Aldrich	Cat #: Y0503

(*Continued on next page*)

Continued

REAGENT or RESOURCE	SOURCE	IDENTIFIER
Critical commercial assays		
ATAC-seq kit	Active motif	Cat #: AT53150
Min Elute PCR Purification kit	Qiagen	Cat #: 28006
TOPscript™ cDNA Synthesis kit	Enzynomics	Cat #: EZ005M
Matrigel® Growth Factor Reduced (GFR) Basement Membrane Matrix	Corning	Cat #: 354230
Deposited data		
scRNA-seq data	Elyada et al., Hosein et al., Krieger et al.[29,30,36]	GSE125588, GSE129455, EGAD00001006448
ChIP-seq data	Dunham et al.	GSE29611
RNA-seq data	This study	GSE223154
ATAC-seq data	This study	GSE223154
Experimental models: Cell lines		
MiaPaca-2	ATCC	Cat #: CRL-1420, RRID: CVCL_0428
PANC-1	ATCC	Cat #: CRL-1469, RRID: CVCL_0480
MPC-1	This paper	N/A
HEK293T	ATCC	Cat #: CRL-3216, RRID: CVCL_0063
Experimental models: Organisms/strains		
C57BL/6J	The Jackson Laboratory	RRID:IMSR_JAX:000664
129S/Sv-Kras^{tm4Tyj}/J	The Jackson Laboratory	RRID:IMSR_JAX:008180
B6.129P2-Trp53^{tm1Brn}/J	The Jackson Laboratory	RRID:IMSR_JAX:008462
Tg(Pdx1-cre/Esr1*)#Dam/J	Dr. Douglas A. Melton	RRID:IMSR_JAX:024968
B6.Cg-Gt(ROSA)26Sor$^{tm9(CAG-tdTomato)Hze}$/J	The Jackson Laboratory	RRID:IMSR_JAX:007909
C57BL/6N-Prmt1$^{tm1a(EUCOMM)Wtsi}$	International Mouse Phenotyping Consortium	RRID:IMSR_WTSI:1539
Oligonucleotides		
shControl	This paper	CAACAAGATGAAGAGCACCAA
shPRMT1 #1	This paper	CCGGCAGTACAAAGACTACAA
shPRMT1 #2	This paper	GTGTTCCAGTATCTCTGATTA
Primers for RT-qPCR (human)	This paper	See Table S3 for details
Primers for RT-qPCR (mouse)	This paper	See Table S4 for details
Recombinant DNA		
pLKO.1 hygro	Addgene	RRID: Addgene_24150
pMD2.G	Addgene	RRID: Addgene_12259
psPAX2	Addgene	RRID: Addgene_12260
Software and algorithms		
GraphPad Prism 9	Prism	https://www.graphpad.com/scientific-software/prism/
Wave Desktop software (v 2.6.3)	Agilent	N/A
R (v 4.1.2)		https://www.R-project.org
SynergyFinder (v 3.8.2)	Zheng et al.	N/A
CompuSyn	Chou et al.	N/A
Biorender		https://biorender.com

RESOURCE AVAILABILITY

Lead contact

Further information and requests for resources and reagents should be directed to and will be fulfilled by the lead contact, Dae-Sik Lim (daesiklim@kaist.ac.kr).

Materials availability

All plasmids, mice, cell lines, and reagents generated in this study are available from the lead contact with a completed Materials Transfer Agreement (MTA).

Data and code availability

- RNA-, ATAC-, and ChIP-seq raw data have been deposited in NCBI's Gene Expression Omnibus and are accessible through accession number GSE223154. This paper analyzes existing, publicly available data. The accession numbers for these datasets are listed in the key resources table.
- This paper does not report original code.
- Any additional information required to reanalyze the data reported in this paper is available from the lead contact upon request.

EXPERIMENTAL MODEL AND STUDY PARTICIPANT DETAILS

Animal studies

Mice were maintained in the specific pathogen-free (SPF) facility of KAIST Laboratory Animal Resource Center and housed under a 12h/12h light/dark cycle, with free access to regular chow and water. All mice were grouped by no more than 5 mice per cage. Mouse experiments were performed with the approval of the IACUC of Korea Advanced Institute of Science and Technology (KAIST) (KA2020-115). *LSL-K-ras*^{G12D}, *Trp53*^{LoxP}, and *R26-tdTomato* mice were purchased from The Jackson Laboratory and described previously.[49–51] *Prmt1* $^{fl/fl}$ mice (Mouse Genome Informatics [MGI]:4432476) were purchased from the International Mouse Phenotyping Consortium (IMPC) and described previously.[13] *Pdx1-CreERT2* mice were provided by Dr. Douglas A. Melton (Harvard University) and described previously.[52] Inducible Cre-mediated gene deletion was achieved by i.p. injection of tamoxifen (Sigma) at a dose of 200 mg/kg bodyweight on three alternate days at 3 to 4 weeks of age. Tamoxifen was dissolved in corn oil (Sigma) at a concentration of 20 mg/mL.

Subcutaneous transplantation and drug treatment

Female C57BL/B6J mice at 5 to 6 weeks of age were injected subcutaneously on each flank with 5 x 10^5 MPC-1 cells suspended in a 1:1 mixture of culture medium and Matrigel. Tumor volume was assessed by measuring two diameters with digital calipers and calculated as $\frac{1}{2}x^2y$, where x is the smaller diameter and y is the larger diameter. When tumors reached a volume of ~200 mm^3, mice were randomized to the various drug treatment groups. Gemcitabine (Sigma) was dissolved in PBS at 10 mg/mL, furamidine (Sigma) in water at 1 mg/mL, and TC-E 5003 (Cayman) in DMSO at 20 mg/mL and further diluted with 1:1 PEG300/saline for injection. Tumor-bearing mice were injected i.p. with gemcitabine at 40 mg/kg once a week, with furamidine at 20 mg/kg twice a week, and TC-E 5003 at 8 mg/kg 5 times a week for 3 weeks. Tumor size was monitored weekly, and experiments were terminated when the tumor volume had increased to ~1500 mm^3.

Cell culture

HEK293T, MiaPaca-2, and PANC-1 cell lines were obtained from the American Type Culture Collection (ATCC). Mouse pancreatic cancer (MPC-1) cells were established from the tumor of a *KP*^{f}*C*^{ER} mouse via outgrowth culture. The tumor was harvested and minced into small pieces with a razor blade. Tissue pieces were washed with PBS and sparsely seeded into a 6-well plate in DMEM supplemented with 10% FBS. Media was changed every 3 days. Once cells spread sufficiently, they were trypsinized and filtered through a 45 μm filter to remove any remaining tissue junks before re-seeding. Single clones were picked via serial dilution and expanded to ensure homogeneity. HEK293T, PANC-1, and MPC-1 cells were maintained in DMEM supplemented with 10% FBS and 1% penicillin-streptomycin, and MiaPaca-2 cells were grown in DMEM supplemented with 10% FBS, 2.5% horse serum, and 1% penicillin-streptomycin. All cells were grown under 5% CO_2 at 37°C. Cell lines were checked for mycoplasma contamination using the MycoStrip Mycoplasma detection kit (Invivogen).

Ex vivo mouse and human patient-derived pancreatic tumor organoid culture

Ex vivo mouse and human patient-derived organoids (PDOs) were performed as previously described.[32,53] In brief, mouse pancreatic tumors were minced into small pieces (~1 mm) with a razor blade and digested with Collagenase (Sigma) and Dispase (Stem Cell Technology) in basal medium at 37°C for 45 min. The disassociated cells were seeded in 40 μL Matrigel (Corning) in a 24-well culture dish, overlayed with complete culture media, and maintained under 5% CO_2 at 37°C. For sectioning, organoids were embedded in Histogel (Thermo Fisher Scientific), fixed in 10% neutral-buffered formaldehyde, and embedded in paraffin. For drug sensitivity assays, identical amounts of cells were seeded, drugs were added after the organoids had fully formed, and maintained in culture for 5 days before further downstream analysis. Human pancreatic cancer patient derived organoids were obtained from the National Cancer Center. Patient sample collection and experimental procedures were approved by the IRB of the National Cancer Center (NCC2021-0232) and by the IRB of KAIST (IRB-23-161).

Tumor microarrays of pancreatic cancer patients

Human pancreatic cancer tissue microarrays were obtained from the National Biobank of Korea at Chonnam National University Hwasun Hospital. Donor patients underwent surgical tumor resections at Chonnam National University Hwasun Hospital between

2004 and 2017. All samples were obtained with written consent and approved by the Institutional Review Board (IRB) of Chonnam National University Hwasun Hospital (CNUHH-2023-013).

METHOD DETAILS

Histology and IHC staining

Mice pancreata were fixed overnight at 4°C in 10% neutral-buffered formalin, embedded in paraffin, sectioned at a thickness of 3 μm with a Leica RM2245 microtome, and stained with H&E (Sigma). For immunostaining, sections were deparaffinized, rehydrated in a series of ethanol solutions of decreasing concentrations, and subjected to antigen retrieval in sodium citrate buffer (10 mM tri-sodium citrate dehydrate, 0.05% Tween 20, pH 6.0) using a microwave for 15 min. For IHC staining, endogenous peroxidase was inactivated by incubation of sections with 3% H_2O_2 for 10 min. Epitope blocking was performed by incubation of slides with either 10% donkey-serum diluted in PBS containing 0.2% Tween 20 (PBS-T) or 5% bovine albumin serum (BSA) diluted in 0.3% PBS-T for 1h at room temperature. Primary antibodies were incubated overnight at 4°C, followed by secondary antibody incubation for 1 h at room temperature. IHC signals were detected with a DAB peroxidase substrate kit (Vector Laboratories), and images were acquired with a Leica DMLB microscope. Immunofluorescence images were acquired with a Zeiss (LSM 800 or LSM 880) confocal microscope. Nuclei were stained with DAPI (Sigma). Slides were mounted using ProLong Gold anti-fade reagent (Invitrogen). Alcian blue staining was performed using the Alcian blue (pH 2.5) Stain Kit (Vector Laboratories).

Immunoblots

Cells were lysed with RIPA buffer (50 mM Tris-Cl (pH 7.5), 150 mM NaCl, 1 mM EDTA, 0.5% deoxycholate, 1% NP-40, and 0.1% SDS) supplemented with protease and phosphatase inhibitors (PMSF, PAFS, leupeptin, and pepstatin). Cell lysates were centrifuged at 13,000 rpm for 10 min at 4°C. The supernatant was collected, protein concentration was measured by Bradford assay, and subjected to SDS-PAGE. The separated proteins were transferred to either nitrocellulose or PVDF membranes, which were subsequently blocked with 5% skim milk in 0.3% PBS-T for 1 h at room temperature. Primary antibodies were incubated overnight at 4°C. Membranes were washed three times with 0.3% PBS-T and incubated with horseradish peroxidase (HRP)-conjugated secondary antibodies for 1 h at room temperature. Signals were detected using ECL reagent (Millipore).

RNAi

DNA fragments encoding shRNAs were cloned into the lentiviral vector pLKO.1 hygro. The target sequences are listed in STAR Methods. HEK 293T cells were transfected with 10 μg of vector DNA, 4 μg psPAX2, and 2 μg pMD2.G using polyethylenimine (PEI). The supernatant containing lentivirus was collected 48 h after transfection and centrifuged at 3,000 rpm for 20 min to remove cell debris. Target cells were infected with the virus in the presence of 8 μg/mL polybrene and selected for at least 3 days in the presence of hygromycin (12.5 μg/mL).

Cell proliferation and colony formation assay

Cell proliferation was measured with a Cyto X cell viability assay kit (LPS Solution). Absorbance at 450 nm was measured with a Versamax microplate reader (Molecular Devices). For the colony formation assay, cells were sparsely seeded in six-well plates, cultured for one week, fixed with methanol and acetic acid (3:1, v/v), and stained with 0.5% crystal violet in methanol. Intensity percent was measured with ImageJ using the ColonyArea plugin.[54,55]

RNA extraction and quantitative real-time PCR

Total RNA was isolated from pancreatic tissue or cultured cells using Hybrid-R (GeneAll), and portions (1.6 μg) of total RNA were subjected to reverse transcription using a TOPscript cDNA Synthesis Kit (Enzynomics). qRT-PCR was performed on a CFX Connect (Bio-rad) using TOPreal SYBR Green qPCR PreMIX (Enzynomics). Either *18S rRNA* or *TBP* was used as endogenous control. The sequences of qPCR primers are listed in Tables S3 and S4.

RNA-seq analysis

RNA libraries were generated using the TruSeq Stranded Total RNA library Prep Gold Kit (Illumina) and sequenced on the Illumina platform. Raw reads were trimmed of adaptor sequences using Trim_galore (v 0.6.7), mapped onto the human reference genome (hg19) using *HISAT2* (v 2.2.1),[56] and assembled into transcripts or genes and quantified using *StringTie* (v 2.2.1).[57] The data were then normalized with *Ballgown* (v 2.26.0), and relative abundance was measured.[58,59] Statistically significant differentially expressed genes were obtained with filtering criteria of $p < 0.05$. GSEAPreranked was performed with GSEA software (v 4.0.3) using gene sets from the molecular signature database (MSigDB) and Kyoto Encyclopedia of Genes and Genomes (KEGG).[60–62] Pathway analysis was performed with EnrichR.[63,64]

Generation of ATAC-seq samples

A suspension of nuclei was prepared according to the Omni-ATAC protocol.[65] In brief, cells were exposed to trypsin and counted to obtain ~100,000 cells per sample using the Active Motif ATAC-seq kit (Active Motif). Cell pellets were suspended in lysis buffer and

centrifuged for 5 min at 4°C. Nuclei were resuspended in transposition buffer and incubated for 30 min at 37°C. Transposed DNA was eluted in 35 μL of buffer using a MinElute PCR purification kit (Qiagen) and amplified by PCR (11 cycles) with Illumina (i7/i5) primers.

ChIP-seq library preparation

Cells were subjected to cross-linking by incubation with 1.5% formaldehyde for 10 min at room temperature, followed by quenching with 0.125 M Glycine for 5 min. Nuclear extracts were sonicated using a Bioruptor (Bio-rad). The sheared nuclear extracts were subjected to immunoprecipitation overnight at 4°C with antibodies or control rabbit IgG bound to Dynabeads protein A (Thermo Fisher Scientific). DNA fragments bound by the antibodies were purified using a MinElute PCR purification Kit (Qiagen), subjected to sequencing library preparation using a TruSeq ChIP-seq Library Prep Kit (Illumina), and sequenced with an Illumina NovaSeq 6000.

Analysis of ATAC-seq and ChIP-seq data

FastQC (v 0.11.9) was applied to examine read quality before alignment and downstream analysis. We used *Trim_galore* (v 0.6.7) to remove reads shorter than 30 bp and aligned the trimmed reads to hg19 using *Bowtie2* (v 2.4.4).[66] Mitochondrial reads, reads without unique alignment, and reads with a mapping quality of <30 were removed using *Samtools* (v 1.14), duplicate reads were removed with *Picard MarkDuplicates* (v 2.26.3) (http://broadinstitute.github.io/picard), and blacklisted regions were filtered out with *BEDtools intersect* (v 2.30.0).[67] Peak calling was performed with *MACS3* (v 3.0.0).[68] The raw counts were globally normalized into CPM. *De novo* motif prediction was performed using *findMotifsGenome.pl* in HOMER software (v 4.11).[69] *Diffbind* was used to identify PRMT1-dependent open chromatin regions.[70] For the annotation of differentially bound sites, *annotatePeaks.pl* in HOMER was applied. The annotated differential peak data for peak locations $FC < -1.5$, with associated p values of 0.05 or less. Genome coverage bigwig files were generated with deeptools2 *bamCoverage* (v 3.5.1).[71] ATAC-seq and ChIP-seq signals were visualized with the Integrative genomic viewer (IGV, v 2.14.1).[72]

Metabolic analyses

Seahorse assays were performed with an XFe96 Extracellular Flux Analyzer (Agilent). In brief, ~2 x 10^4 MiaPaca-2 and ~1 x 10^4 PANC-1 cells were seeded, and the oxygen consumption rate (OCR), extracellular acidification rate (ECAR), and proton efflux rate (PER) were measured. 0.5 μM Rotenone/antimycin A (Rot/AA) and 100 mM 2-deoxyglucose (2-DG) were administered to the cells for the glycolytic rate assay, and 1 μM oligomycin (Oligo), 1 μM fluoro-carbonyl cyanide phenyl-hydrazone (FCCP), and 0.5 μM Rot/AA were administered for the mitostress assay. Seahorse results were normalized by protein concentration and analyzed with Wave Desktop software (Agilent, v 2.6.3). Statistics and graphical representations were performed in Prism 9.0 (Graph pad).

Analysis of public datasets

Single cell RNA sequencing data were downloaded from the Gene Expression Omnibus (GEO) and Zenodo (5552404) and analyzed with *Seurat* (v4.2.0) in *R* (v 4.1.2) using Rstudio.[73] Analysis of TCGA datasets was performed with cBioportal and GEPIA.[74,75] H3K27ac and H3K4me3 ChIP-seq data were downloaded from the ENCODE portal (ENCSR000AMZ).

Synergy prediction

For synergy analysis, individual values of relative cell viability from each well were measured and analyzed using the SynergyFinder package (v 3.8.2) in R.[76] Synergy scores < -10, from -10 to 10, and >10 indicate an antagonistic, additive, and synergistic effect, respectively. The effect of the combination of gemcitabine and furamidine was evaluated using CompuSyn software.[77] $CI < 1$, $CI = 1$, and $CI > 1$ indicate a synergistic, additive, and antagonistic effect, respectively. The synergistic effect of both drugs was determined with synergy score and CI value.

QUANTIFICATION AND STATISTICAL ANALYSIS

All statistical analyses were performed using GraphPad Prism 9.0. Statistical analyses other than two-tailed unpaired Student's *t*-tests are indicated in the figure legends. In brief, one-way ANOVA with either Dunnett's multiple-comparison tests or Tukey's multiple-comparison tests were used to compare data points of more than two groups. The log rank (Mantel-Cox) test was used for the comparison of survival curves, and two-way ANOVA with correction for multiple comparisons with the Tukey, Bonferroni, or Holm-Šídák method was adopted for the comparison of seahorse plots, area of transformed lesions, and tumor growth curves, respectively. Quantitative data are presented as means ± SEM. A p value of <0.05 was considered statistically significant.